Advances in Water Resources 86 (2015) 240–255

Contents lists available at ScienceDirect

Advances in Water Resources

journal homepage: www.elsevier.com/locate/advwatres

Wind-induced leaf transpiration

Cheng-Wei Huang [a,*], Chia-Ren Chu [b], Cheng-I Hsieh [c], Sari Palmroth [a,d], Gabriel G. Katul [a,e]

[a] Nicholas School of the Environment, Duke University, Durham, NC, USA
[b] Department of Civil Engineering, National Central University, Taoyuan, Taiwan
[c] Department of Bioenvironmental Systems Engineering, National Taiwan University, No. 1, Section 4, Roosevelt Road, Taipei 10617, Taiwan
[d] Department of Forest Ecology and Management, Swedish University of Agricultural Sciences, SE-901 83 Umeå, Sweden
[e] Department of Civil and Environmental Engineering, Duke University, Durham, NC, USA

ARTICLE INFO

Article history:
Received 21 July 2015
Revised 12 October 2015
Accepted 16 October 2015
Available online 24 October 2015

Keywords:
Energy balance
Laminar boundary layer
Leaf-level gas exchange
Optimality hypothesis
Wind effects

ABSTRACT

While the significance of leaf transpiration (f_e) on carbon and water cycling is rarely disputed, conflicting evidence has been reported on how increasing mean wind speed (U) impacts f_e from leaves. Here, conditions promoting enhancement or suppression of f_e with increasing U for a wide range of environmental conditions are explored numerically using leaf-level gas exchange theories that combine a stomatal conductance model based on optimal water use strategies (maximizing the 'net' carbon gain at a given f_e), energy balance considerations, and biochemical demand for CO_2. The analysis showed monotonic increases in f_e with increasing U at low light levels. However, a decline in modeled f_e with increasing U were predicted at high light levels but only in certain instances. The dominant mechanism explaining this decline in modeled f_e with increasing U is a shift from evaporative cooling to surface heating at high light levels. New and published sap flow measurements for potted *Pachira macrocarpa* and *Messerschmidia argentea* plants conducted in a wind tunnel across a wide range of U ($2-8$ m s^{-1}) and two different soil moisture conditions were also employed to assess how f_e varies with increasing U. The radiative forcing imposed in the wind tunnel was only restricted to the lower end of expected field conditions. At this low light regime, the findings from the wind tunnel experiments were consistent with the predicted trends.

1. Introduction

The global water and carbon cycle sensitivity to stomata predicted by global climate models that employ the Ball-Berry [3] or Leuning [44] stomatal conductance formulations has been convincingly documented [6,13,21]. Likewise, detailed ecosystem models predicting gas exchange between the biosphere and atmosphere are analyzed in terms of their sensitivity to stomatal conductance [1,37]. Since water loss through stomata (i.e., transpiration) to the dry atmosphere is inevitable when CO_2 uptake (i.e., assimilation) occurs, how stomata respond to environmental factors has long been an active research area. Environmental factors governing transpiration (f_e) from leaves include, at minimum, atmospheric CO_2 concentration (c_a), air temperature (T_a), air relative humidity (RH) or vapor pressure deficit (VPD), photosynthetically active radiation (PPFD), soil moisture (or leaf water potential) and mean wind speed (U) [52]. When surveying the literature encompassing a wide range of ecosystems and environmental conditions, conflicting empirical results on the sign of $\partial f_e/\partial U$ emerged [7,10,11,17,23–25,28,30,31,39,49,63]. Positive, negative or week dependency of f_e on U for numerous forested canopies has been highlighted and discussed elsewhere [39]. This is perhaps not surprising and has been foreshadowed by Monteith [52] who pointed out that wind effects on f_e are a vexing problem because of their non-monotonic effects. The thickness of the laminar boundary layer pinned to a leaf surface, which monotonically depends on U, determines the diffusive path length for the exchanges of gases between the leaf surface and the turbulent atmosphere above the laminar boundary layer. However, U also dictates the heat exchange between leaves and the overlying atmosphere as well as the degree of evaporative cooling experienced at the leaf surface depending on the radiation load.

The Penman–Monteith (PM) equation that utilizes an energy balance has been extensively used to predict f_e for more than 50 years in hydrology. The dependence of f_e on U was discussed in the original work describing the PM equation, indicating that the sign of $\partial f_e/\partial U$ is mainly governed by a competition between evaporative cooling and surface heating (or cooling). However, the biotic controls for water transport through the stomatal pathway (i.e., encoded as stomatal conductance g_s here) remain weakly dependent on U

* Corresponding author. Tel.: +1 919 536 8252.
E-mail addresses: cheng.wei.huang@duke.edu, ch224@duke.edu (C.-W. Huang), crchu@ncu.edu.tw (C.-R. Chu), hsieh@ntu.edu.tw (C.-I. Hsieh), sari.palmroth@duke.edu (S. Palmroth), gaby@duke.edu (G.G. Katul).

http://dx.doi.org/10.1016/j.advwatres.2015.10.009
0309-1708/

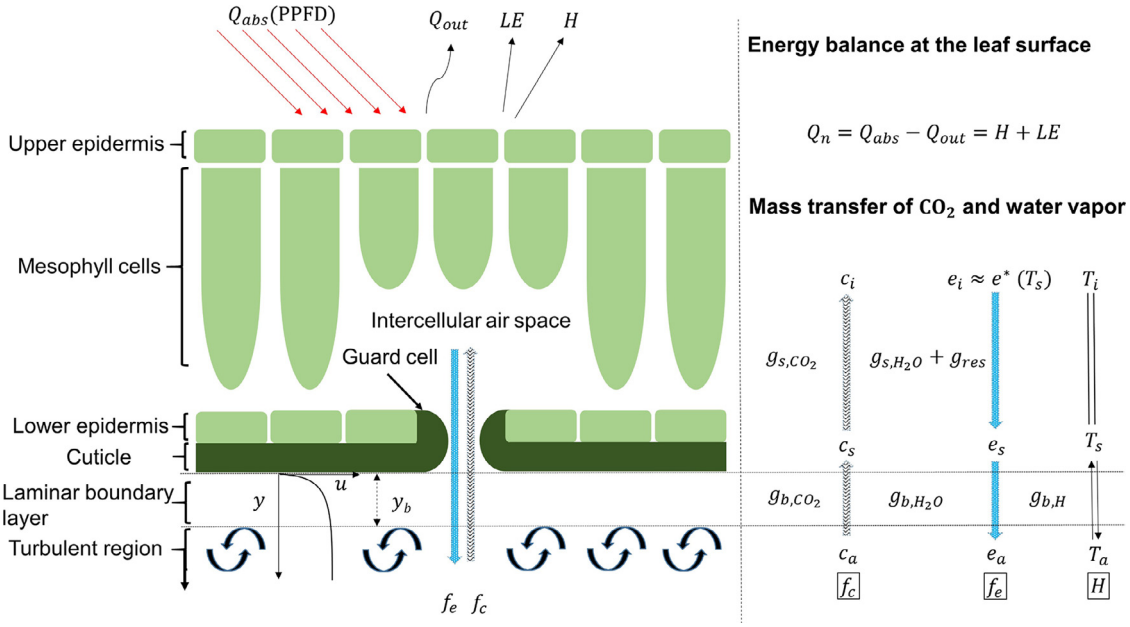

Fig. 1. Schematic of the mass (CO_2 and water vapor) and energy transfer between the leaf and the atmosphere. Note that u is the average wind velocity at the distance y from leaf surface within the laminar boundary layer and y_b is the thickness of the laminar boundary layer.

in the PM equation. To be clear, gas exchange through stomata of biologically active scalars is a complex problem given the biotic controls imposed by guard cells. The stomatal pathway serves as the main conduit for CO_2 and water vapor exchange, but this pathway can be further impacted by the laminar boundary layer (see Fig. 1). Thus, the main objective of this work is to disentangle wind effects from other exogenous environmental factors (e.g., radiative cooling) on g_s and f_e so as to explore the manifold of possible conditions promoting $\partial f_e/\partial U$ to reverse from > 0 to < 0 with increasing U.

When analyzing responses of stomata to their environment, temperature, atmospheric CO_2 concentration and water vapor pressure at the leaf surface are commonly assumed to be sufficiently close to their counterparts in the atmosphere represented by their states beyond the outer edge of the laminar boundary layer. A plausible argument for this approximation is that the thickness of the laminar boundary layer pinned to a leaf is sufficiently small so that the leaf is presumed to be 'well-coupled' to its environment. This approximation is common when interpreting leaf-gas exchange measurements in cuvettes where the flow rate through the chamber is sufficiently large to ensure the validity of the 'well-coupled' approximation. This approximation becomes also convenient when deriving relations between g_s and external environmental conditions [20]. Following this 'approximation', only monotonic increase in f_e with increasing U (i.e., $\partial f_e/\partial U > 0$ for increasing U) is expected primarily due to the reduced thickness of the laminar boundary layer. Because measurements (e.g., g_s) within such thin and disturbed laminar boundary layer adjacent to the leaf experiencing variable U are difficult to conduct, a leaf-level gas exchange model is needed and developed here for computing mass transfer of CO_2 and water vapor. The model combines biochemical demand for CO_2 as described by the Farquhar photosynthesis model [19] for C3 plants, a Fickian mass transfer including transfer through the laminar boundary layer that may be experiencing forced or free convection depending on U and the radiation load, an optimal leaf water use strategy that maximizes 'net' carbon gain for a given f_e describing stomatal aperture variations, and a leaf-level energy balance to accommodate evaporative cooling. Hence, the proposed model is able to bridge the gap between biological controls through stomata and the aerodynamic modifications due to U as may be experienced in natural settings. These calculations can be used to arrive at a closed set of equations that predict f_e through g_s as impacted by variable U. The manifold of conditions promoting the sign reversal of $\partial f_e/\partial U$ with increasing U can therefore be numerically delineated.

To address this study objective, the manuscript is organized as follows. The model development is first presented in Sections 2.1 and 2.2 featuring the mass transfer equations for water and carbon dioxide gases through stomates and through the laminar boundary layer. The Farquhar photosynthesis model applied to the mesophyll and the energy balance at the leaf surface are then presented in Sections 2.3 and 2.4, respectively and then coupled to the mass transfer equations. The optimality hypothesis for stomatal aperture variations with variations in environmental conditions, which is used to mathematically close the overall set of equations for the model system, is discussed in Section 2.5. Other 'closure' conditions for stomatal aperture variations such as those widely used in land-surface schemes (e.g. a Ball-Berry or Leuning type closure) are briefly presented and elaborated on in an appendix. The goal of exploring these alternative and widely used stomatal conductance models is to highlight the non-linearities in $\partial f_e/\partial U$ with increasing U in such g_s model closure. A broad range of environmental conditions (mainly PPDF, soil moisture, and atmospheric humidity) are then explored in Sections 3.1.1–3.1.4 using the proposed model so as to unfold the possible environmental conditions above the laminar boundary layer promoting a sign reversal in $\partial f_e/\partial U$ from > 0 to < 0. Because the work here employs published and recent wind tunnel experiments on potted plants aimed at discerning the effects of U on measured f_e, these experimental conditions and the parameters required in model calculations are used as a case study for the model and are discussed in Section 3.2. The measured dependence of f_e on U at low PPFD is presented in Sections 3.2.1 and 3.2.2 using the published and new sap flow measurements conducted for two different potted plants with similar leaf dimensions in the wind tunnel across a wide range of U and for two different soil moisture states. The wind-tunnel setup has been described elsewhere [11] and only salient features of the experiment are summarized in Appendix A. Since physiological parameters and total leaf area for the potted plants were not directly measured in these wind tunnel experiments, comparisons between modeled and actual leaf-level f_e cannot be directly conducted (discussed later). However, the

relative response of the sap flow measurements to U and their comparison to model calculations can be used to illustrate the behavior of f_e with varying U when all other external conditions are set.

2. Theory

The notation and units used throughout are listed in Appendix B and the mass exchange processes at the leaf scale are featured in Fig. 1. It is assumed that the state variables such as air temperature, CO_2 and water vapor concentrations above the laminar boundary layer (denoted as the turbulent region) are 'well-mixed' and their vertical variations relative to those experienced across the laminar boundary layer are small. The energy driving the system is generated through a pre-set PPFD value incident to the leaf surface. The mean wind speed is externally imposed but decays to zero (i.e. no slip) at the leaf surface over a distance defining the laminar boundary layer thickness. The analysis only applies after steady-state conditions in U and f_e are attained.

2.1. Fickian mass transfer

A two layer mass transport model describing the simultaneous transfer of CO_2 and water vapor across the sub-stomatal cavity and the laminar boundary layer attached to the leaf surface (see Fig. 1) is given as

$$\begin{aligned} f_c &= g_{t,CO_2}(c_a - c_i) \\ f_e &= g_{t,H_2O}(e_i - e_a), \end{aligned} \tag{1}$$

where f_c is the CO_2 flux, f_e is, as before, the water vapor flux, c_a is ambient (or external) and c_i is the inter-cellular CO_2 concentration, e_a is ambient (or external) and e_i is inter-cellular water vapor pressures, g_{t,CO_2} and g_{t,H_2O} are the total conductances at the 'leaf scale' for CO_2 and water vapor, respectively. Here, storage effects in the leaf and laminar boundary layer are assumed to be small or negligible so that the same mass fluxes cross the stomata and the laminar boundary layers at steady state. Also, turbulent conditions away from the laminar boundary layer prevail thereby allowing variations in c_a and e_a to be ignored far from the outer edge of the leaf boundary layer as earlier noted. The g_{t,CO_2} and g_{t,H_2O} can be formulated as

$$\begin{aligned} g_{t,CO_2} &= \frac{g_{s,CO_2} g_{b,CO_2}}{g_{s,CO_2} + g_{b,CO_2}} \\ g_{t,H_2O} &= \frac{(g_{s,H_2O} + g_{res}) g_{b,H_2O}}{g_{s,H_2O} + g_{res} + g_{b,H_2O}} \end{aligned} \tag{2}$$

where g_{s,CO_2} and $g_{s,H_2O} (\approx 1.6 g_{s,CO_2})$ are respectively the stomatal conductance to CO_2 and water vapor [32], g_{res} is the 'residual conductance', and g_{b,CO_2} and g_{b,H_2O} are respectively the boundary layer conductance for CO_2 and water vapor including both forced and free convection. These boundary layer conductances can be determined from U and temperature difference (δT) between the leaf surface (T_s) and the atmosphere away from the laminar boundary layer (T_a) as well as the characteristic dimension of the leaf (d) as described elsewhere [9]. To determine f_e and f_c, g_{t,CO_2} and g_{t,H_2O} are required. The following sections describe the determination of $g_{b,i}$ (that varies with U and $\delta T = T_s - T_a$) and $g_{s,i}$ where i refers to CO_2, H_2O or sensible heat (H). As shown by several experiments [8,15,54], nocturnal transpiration need not be zero and can be attributed to a combined effect of water loss from stomata (minor leakage from guard cells) and cuticle. This additional water loss typically constitutes 10–30% of daily transpiration but is not regulated by the biochemical demand of CO_2. Thus, g_{res} in Eq. (2) must be interpreted as the sum of night-time (i.e., modeled by setting PPFD=0) stomatal g_{night} and cuticular g_{cut} conductance without distinguishing between them. Eq. (2) also assumes that the mesophyll conductance to CO_2 is much larger than its stomatal counterpart though these mesophyll effects can be included if known (e.g., [60]). Hence, when using Eq. (1), a point of departure from previous models is that well-coupled conditions between the leaf and the atmosphere (i.e., $f_c \approx g_{s,CO_2}(c_a - c_i)$ and $f_e \approx g_{s,H_2O}\mathrm{VPD}$) are not assumed as the laminar boundary layer thickness changes with changing U as well as leaf surface heating or cooling. It is for this reason that previous models using this approximation predict only increasing f_e with increasing U and a constant g_{s,CO_2} independent of U (see Appendix C).

2.2. Boundary layer conductances for heat and mass transfer in forced and free convection

For heat and mass transfer within the laminar boundary layer adjacent to the leaf surface, the combined effects of forced and free convection can be expressed as:

$$g_{b,i} = 1.4 g_{b,i,forced} + g_{b,i,free} \tag{3}$$

where $g_{b,i}$ is the boundary layer conductance, $g_{b,i,forced}$ and $g_{b,i,free}$ are respectively the forced and free convection conductances. The factor of 1.4 is adopted for naturally turbulent flow as suggested elsewhere [9]. Through the connection to U, d and δT (the temperature difference across the laminar boundary layer reflecting $T_s - T_a$), the empirical formulations of $g_{b,H,forced}$ and $g_{b,H,free}$ are given as [9]:

$$\begin{aligned} g_{b,H,forced} &= \frac{0.664 \rho D_H Re^{1/2} Pr^{1/3}}{d}, \\ g_{b,H,free} &= \frac{0.54 \rho D_H (GrPr)^{1/4}}{d}, \end{aligned} \tag{4}$$

where ρ is the mean air molar density, D_H is the thermal diffusivity, $Re = (Ud)/\nu$ is the Reynolds number, where ν is the air kinematic viscosity, $Pr = \nu/D_H$ is the Prandtl number, and $Gr = (gd^3\delta T)[(T_a + 273.15)\nu^2]$ is the Grashof number, where g is the gravitational acceleration. The forced and free convection conductances for CO_2 and water vapor can be determined by substituting D_H and Pr in Eq. (4) with their molecular diffusivity D_i and Schmidt number S_c, respectively. A leaf-level energy balance (see Section 2.4) is now required to determine the unknown variable T_s (or δT).

2.3. Farquhar photosynthesis model

For C3 species, the biochemical demand for CO_2 is commonly described by the C3-photosynthesis model [19]. Here, this biochemical demand is approximated by a hyperbolic function reflecting the co-limitations of Rubisco activity and ribulose-1,5-biphosphate (RuBP) regeneration rate (and hence electron transport) on photosynthesis and is given as [59]:

$$\begin{aligned} f_c &= \frac{k_1 (c_i - \Gamma^*)}{k_2 + c_i} - R_d \\ k_1 &= \frac{J}{4} \\ k_2 &= k_1 \frac{a_2}{V_{c,max}} \end{aligned} \tag{5}$$

where k_1 and k_2 are associated with the photosynthetic parameters, Γ^* is the CO_2 compensation point in the absence of mitochondrial respiration, R_d is the daytime mitochondrial respiration rate, J is the electron transport rate that varies with PPFD and the light saturated rate of electron transport (J_{max}) as described elsewhere [51,59], $a_2 = K_c(1 + C_{oa}/K_o)$, where K_c and K_o are the Michaelis constants for CO_2 fixation and oxygen inhibition and C_{oa} is the ambient oxygen concentration, and $V_{c,max}$ is the maximum carboxylation capacity. A feature of this representation is that the abrupt transition between Rubisco-limited and RuBP-limited photosynthesis is bypassed without requiring an additional *ad hoc* curvature parameter. This form of the biochemical demand for CO_2 ensures that at low c_i, $V_{c,max}$ appreciably controls photosynthesis. Conversely, at large c_i, J_{max} limits

Table 1
Physiological parameters and their temperature adjustments for biochemical model [9].

Parameters	Value or temperature adjustment	Unit
$V_{cmax,25}$[a]	50	μ mol m^{-2} s^{-1}
$J_{max,25}$[a]	100	μ mol m^{-2} s^{-1}
$K_{c,25}$	300	μ mol mol^{-1}
$K_{o,25}$	300	mmol mol^{-1}
C_{oa}	210	mmol mol^{-1}
$V_{c,max}$	$V_{cmax,25}\frac{\exp[0.088(T_s-25)]}{1+\exp[0.29(T_s-41)]}$	μ mol m^{-2} s^{-1}
J_{max}[b]	$J_{max,25}\exp[\frac{160(T_s-25)}{298RT_s}]$	μ mol m^{-2} s^{-1}
K_c	$K_{c,25}\exp[0.074(T_s-25)]$	μ mol mol^{-1}
K_o	$K_{o,25}\exp[0.018(T_s-25)]$	mmol mol^{-1}
τ	$2.6\exp[-0.056(T_s-25)]$	mmol mol^{-1}
Γ^*	$\frac{C_{oa}}{2\tau}$	μ mol mol^{-1}

[a] The values of $V_{cmax,25}$ and $J_{max,25}$ were taken to be within the range of the data reported elsewhere [61,62].
[b] The formulations of J_{max} and $V_{c,max}$ dependent on the normalized $J_{max,25}$ and $V_{cmax,25}$ at 25 °C were adopted from elsewhere [4,9,51].

photosynthesis. The parameters of the biochemical demand model and their temperature adjustments are summarized in Table 1. Combining Eqs. (1) and (5), c_i and f_c can be expressed as a function of g_{t,CO_2} and photosynthetic parameters using [36]:

$$\frac{c_i}{c_a} = \frac{1}{2} + \frac{1}{2g_{t,CO_2}c_a}[-k_1 - k_2 g_{t,CO_2} + R_d + \sqrt{\left[k_1 + (k_2 - c_a)g_{t,CO_2} - R_d\right]^2 - 4g_{t,CO_2}\left(-c_a g_{t,CO_2}k_2 - k_2 R_d - k_1\Gamma^*\right)}] \quad (6)$$

and

$$f_c = \frac{1}{2}[k_1 + (k_2 + c_a)g_{t,CO_2} + R_d - \sqrt{\left[k_1 + (k_2 - c_a)g_{t,CO_2} - R_d\right]^2 - 4g_{t,CO_2}\left(-c_a g_{t,CO_2}k_2 - k_2 R_d - k_1\Gamma^*\right)}]. \quad (7)$$

From Eqs. (6) and (7), it is evident that c_i and f_c (i.e., the biochemical demand for CO_2) are impacted by the laminar boundary layer through g_{t,CO_2} (see Eq. 2) when accounting for the aerodynamic changes induced by changes in U. The laminar boundary layer bridging the atmosphere to the leaf surface may be substantially altered when the leaf is decoupled from the atmosphere given that f_c, f_e and H are respectively connected to c_a, e_a and T_a through $g_{b,i}$ (see Fig. 1) and photosynthetic parameters that depend on T_s (not T_a). Two additional formulations are now required to solve for g_{s,CO_2} and T_s assuming g_{res} can be *a priori* estimated.

2.4. Energy balance at the leaf scale

When the specific heat capacity of the leaf is assumed to be minor and can be ignored, the leaf energy balance under steady-state conditions can now employed to determine T_s and is given as [9]:

$$\begin{aligned} Q_n &= Q_{abs} - Q_{out} = H + LE \\ Q_{out} &= \epsilon_s\sigma(T_s + 273.15)^4 \\ H &= c_p g_{b,H}(T_s - T_a) \\ LE &= Lf_e/P_a, \end{aligned} \quad (8)$$

where the net radiation (Q_n) is computed from the difference between the absorbed radiation (Q_{abs}) and emitted longwave radiation (Q_{out}) balanced by H and latent heat (LE) fluxes on the leaf surface, ϵ_s is the leaf surface emissivity, σ is the Stefan-Boltzmann constant, c_p is the specific heat capacity of dry air at constant pressure, L is the latent heat of vaporization of water, $g_{b,H}$ is the boundary layer conductance for heat in forced and free convection (see Section 2.2), and P_a is the atmospheric pressure. The Q_{abs} can be determined from PPFD measurements assuming a constant ratio of all-wave Q_{abs} to incident PPFD as suggested elsewhere [27]. The T_s is now computed as:

$$T_s = T_a + \frac{Q_{abs} - \epsilon_s\sigma(T_s + 273.15)^4 - Lg_{t,H_2O}(e_i - e_a)/P_a}{c_p g_{b,H}} \quad (9)$$

where $e_i \approx e^*(T_s)$ given that the water vapor pressure in the intercellular air space is nearly saturated at temperature $T_i = T_s$ (see Fig. 1). It is to be noted that T_s is determined here without invoking any linearization, which is a departure from the assumptions used in the original PM derivation. However, a numerical scheme for solving T_s is now required as T_s is retained on the right hand side of Eq. (9) (also embedded in g_{t,H_2O} and $g_{b,H}$). Eqs. (8) and (9) again show the significance of the aerodynamic modifications introduced by U through $g_{b,i}$ contributing to H (or T_s) and LE. Also, the derivation here assumes that $g_{b,i} > 0$, which necessitates a $U > 0$. The partitioning of the leaf energy balance to H or LE is also connected to the biochemical demand for CO_2 and optimal water use (discussed later) as shown in Sections 2.1 and 2.5.

2.5. Optimality hypothesis for stomatal aperture variations

To close the system of equations, a number of models have been proposed as independent expressions for g_{s,CO_2} (see review by Damour et al. [14]). Here, an optimality hypothesis [5,12,22,29,41] that uses the economics of leaf-gas exchange is selected in lieu of the widely used Ball-Berry [3] (superscripted as BB) or Leuning [44] (superscripted as LEU) semi-empirical models. According to this hypothesis, the short-term regulation of stomatal aperture is achieved by maximizing carbon gain constrained by water availability or water loss (i.e., f_e). This constrained optimization is mathematically equivalent to an unconstrained optimization problem using an objective function (or Hamiltonian) defined as

$$h_a(g_{s,CO_2}) = f_c - \lambda f_e, \quad (10)$$

where the species-specific cost of water parameter λ is known as the marginal water use efficiency and measures the cost to the plant of loosing water in carbon units thereby bridging the carbon and water economies of the plant. Mathematically, λ is the Lagrange multiplier for the unconstrained optimization problem. Assuming λ is approximately constant on time scales commensurate with stomatal aperture fluctuations but it can vary on longer time scales [48], the optimal g_{s,CO_2} can be determined by setting

$$\frac{\partial h_a(g_{s,CO_2})}{\partial g_{s,CO_2}} = \frac{\partial f_c}{\partial g_{s,CO_2}} - \lambda\frac{\partial f_e}{\partial g_{s,CO_2}} = 0, \quad (11)$$

with $\lambda = (\partial f_c/\partial g_{s,CO_2})/(\partial f_e/\partial g_{s,CO_2}) = b^2 > 0$, where b is constant over time scale over which g_{s,CO_2} rapidly varies. Formulated in this manner, g_{s,CO_2} must be 'numerically' computed. Analytical formulation for g_{s,CO_2} can be derived when additional assumptions are proposed including $g_{t,CO_2} \approx g_{s,CO_2}$ or when $g_{b,CO_2} \gg g_{s,CO_2}$ and the leaf is well coupled to the atmosphere as proposed elsewhere [36] and shown in Appendix C. Upon further assumption of a constant long-term c_i/c_s and a linearized biochemical demand function, the analytical form of g_{s,CO_2} derived from the optimality hypothesis has been shown to be identical to BB and LEU (see Appendix D) except for the reduction function of VPD or RH [37]. When exploring the manifold of possible conditions promoting $\partial f_e/\partial U$ to reverse from > 0 to < 0 with increasing U, the BB and LEU formulations are also employed instead of the optimality hypothesis and the outcomes of these calculations are presented separately in Appendix D but highlighted in the results section.

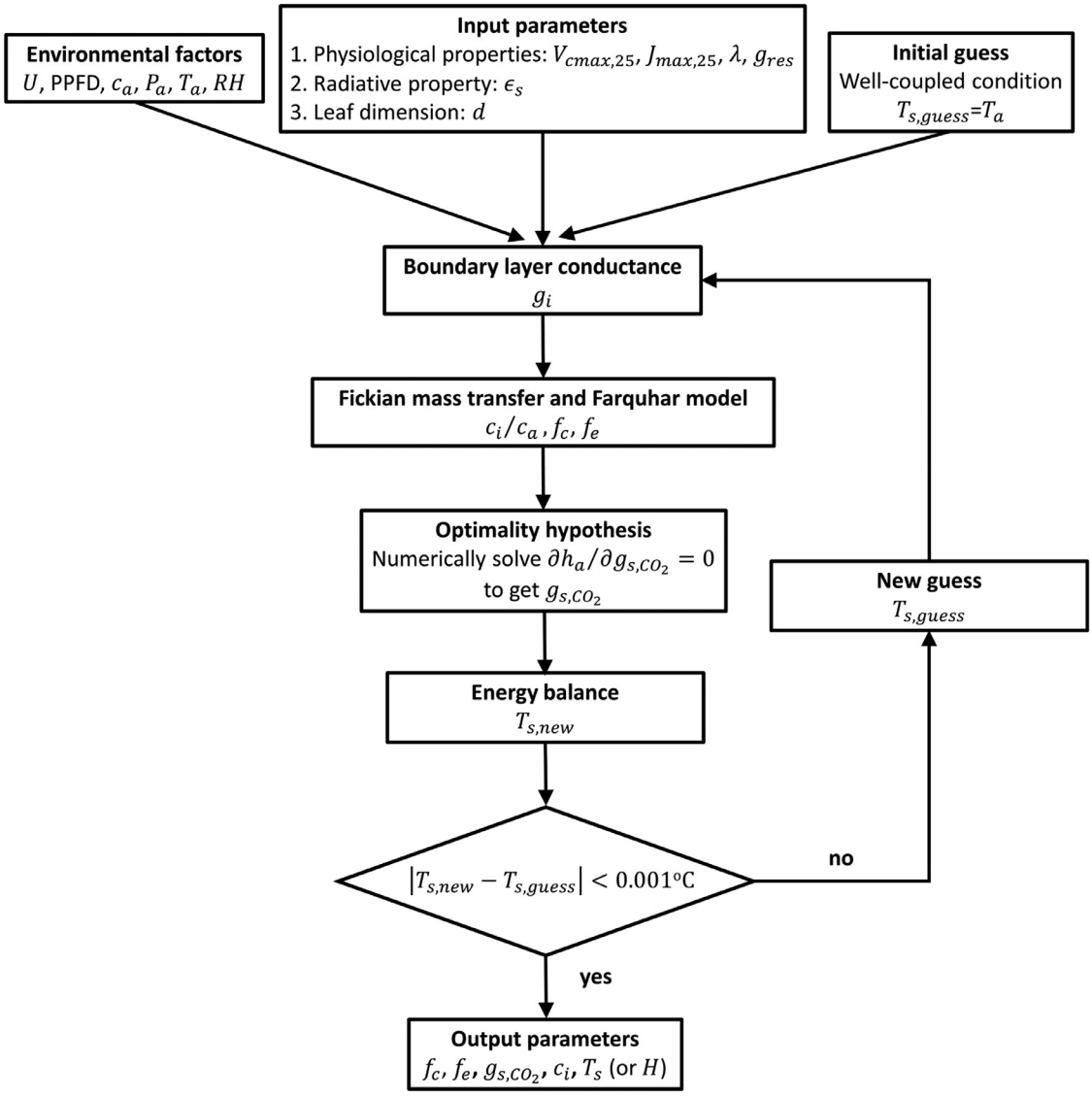

Fig. 2. Flowchart of numerical calculation process for the model system.

As shown in Fig. 2, a numerical solution is now required to determine g_{s,CO_2} and T_s as well as f_c, f_e, and H for a given set of external variables U, Pa, PPFD, Q_{abs}, T_a, e_a (or RH), c_a and leaf dimension d, given that the laminar boundary layer may play a significant role on leaf-level gas exchange. The following parameters are needed to conduct the model calculations: $V_{c,max}$, J_{max}, λ and ϵ_s. The analysis here also assumed that $\partial g_{res}/\partial g_{s,CO_2}=0$ thereby necessitating an independent estimate of g_{res} to complete the mathematical description as earlier noted.

3. Results and discussions

To address the study objective, four scenarios are examined through model calculations to explore the effects of soil water availability and evaporative demand on leaf-level gas exchange across a wide range of wind speed and light availability. These scenarios are for (1) well-watered soil conditions with small evaporative demand, (2) water-stressed soil conditions with small evaporative demand, (3) large evaporative demand under well-watered soil moisture conditions and (4) large evaporative demand under water-stressed soil moisture conditions. These model results are then contrasted with sap flow velocity measurements for a wide range of U but two different soil moisture states reported in previous wind-tunnel experiments [11] and a recent one with a similar configuration described in Appendix A. A drawback in these experiments is that the artificial light used to generate a steady PPFD in the wind-tunnel experiments only corresponds to a low value encountered in natural settings (about a factor of 5–6 lower than the maximum theoretical PPFD for clear-sky conditions).

3.1. Model analysis illustrating a decreasing f_e with increasing U

Prior to discussing the effects of U on leaf-level gas exchange, the difference between the 'actual' evaporative demand and evaporative demand approximated by VPD requires clarification. VPD is the difference between actual and saturated water vapor pressure in the atmosphere (i.e., VPD$= e_a^*(T_a) - e_a = e_a^*(T_a)(1-RH)$), where $e_a^*(T_a)$ is the saturated water vapor pressure at a given ambient temperature outside the laminar boundary layer and can be determined from atmospheric RH and T_a. However, VPD may substantially deviate from the 'actual' evaporative demand (i.e., $e_i - e_a$), which is impacted by wind speed above the leaf surface (see Fig. 1). The deviation between these two evaporative demands increases when the leaf becomes 'decoupled' from the atmosphere (i.e., $T_s \neq T_a$ and

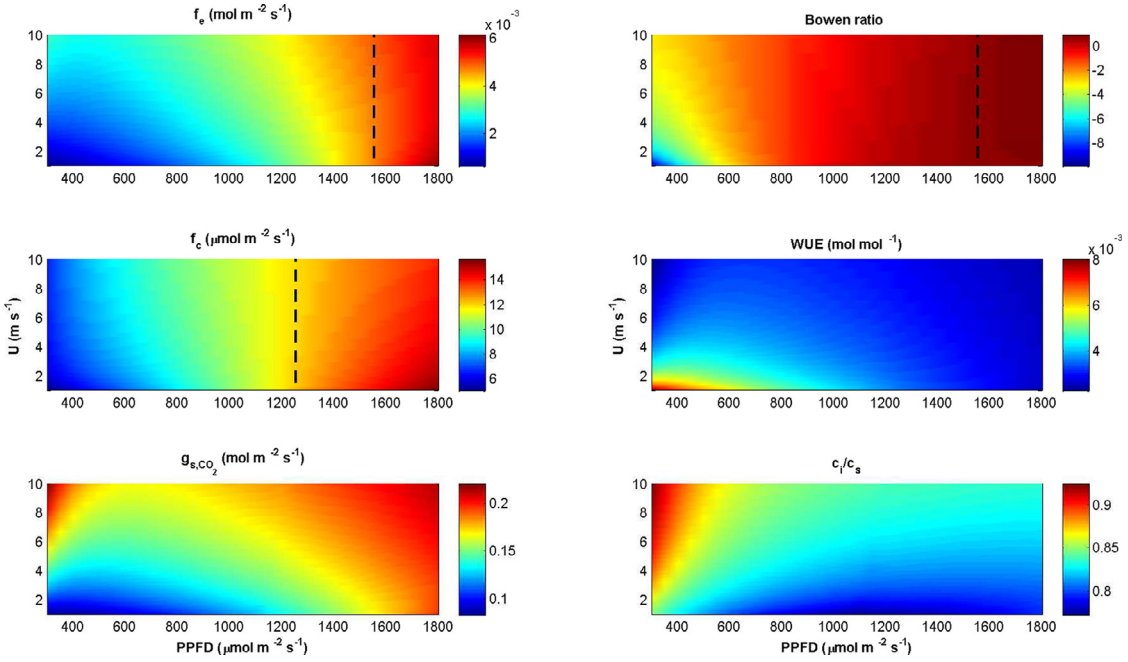

Fig. 3. Modeled transpiration rate (f_e), assimilation rate (f_c), stomatal conductance (g_{s,CO_2}), Bowen ratio (H/LE), WUE (f_c/f_e) and the ratio of the inter-cellular to leaf-surface CO_2 concentration (c_i/c_s) as a function of wind speed (U) and photosynthetically active radiation (PPFD) for well-watered soil condition ($\lambda = 0.001$ μ mol mol^{-1} kPa^{-1}) and small evaporative demand ($RH = 60\%$). Note that the transition PPFD for the reversal sign of $\partial f_e/\partial U$ and $\partial f_c/\partial U$ are 1550 and 1250 μ mol m^{-2} s^{-1} and represented by the broken lines, respectively. The broken line for Bowen ratio (≈0.75) represents the corresponding transition for f_e.

thus $e_i \neq e_a^*(T_a)$) as expected. For the purposes here, VPD (or RH) outside the laminar boundary layer is used to define the dryness of the atmosphere because this measure is not sensitive to U and because it is commonly 'imposed' on the canopy by much larger scale meteorological conditions. The $RH = 60\%$ and 20% were respectively set for small and large atmospheric evaporative demand in model calculations. The PPFD range explored here is selected to be within the expected range of diurnal variations observed in field conditions. All other environmental factors (i.e., $T_a = 25$ °C, $c_a = 400$ ppm and $P_a = 101.3$ kPa), physiological parameters (i.e., $V_{cmax,25}$ and $J_{max,25}$ are respectively 50 and 100 μ mol m^{-2} s^{-1}, which are well within the range in a literature survey encompassing more than 100 species [61,62]), leaf attributes (i.e., d=0.015 m) and $\epsilon_s = 0.95$ are maintained constant. It should be noted that the overall features for the following discussions (i.e., Section 3.1.1–3.1.4) associated with the model calculations are not altered by the choice of the two physiological parameters. While a larger value of λ is expected for limited soil water availability [37,46,47], the values of λ selected for well-watered and water-stressed conditions are respectively 0.001 and 5 μ mol mol^{-1} kPa^{-1} to represent two extreme water conditions in the soil. The value of g_{res} is set to be 0.04 mol m^{-2} s^{-1} but the analysis is not sensitive to g_{res} when it resides in the range from 0.02 to 0.1 mol m^{-2} s^{-1} (not shown here). This range covers values reported for many species as summarized elsewhere [8]. The modeled f_e, f_c and g_{s,CO_2} as well as a number of dimensionless ratios such as the Bowen ratio ($= H/LE$), leaf flux-based water use efficiency (WUE$= f_c/f_e$) and c_i/c_s are shown in Figs. 3–6 for the four scenarios and for increasing U.

3.1.1. Well-watered conditions with small evaporative demand

Fig. 3 shows that f_e, f_c and g_{s,CO_2} generally increase with increasing PPFD as expected. How the trend of f_e, f_c and g_{s,CO_2} is impacted by U clearly varies for different light conditions. Based on the model calculation, $\partial f_e/\partial U > 0$ at lower PPFD while $\partial f_e/\partial U < 0$ at higher PPFD. The transition occurs at PPFD ≈ 1550 μ mol m^{-2} s^{-1} and can be explained by how the energy balance is partitioned between H and LE as U increases. The $\partial f_e/\partial U > 0$ with increasing U occurs when the Bowen ratio < 0. For a small Bowen ratio, H further decreases (i.e., $H < 0$; surface cooling) with increasing U (i.e., $g_{b,H}$) at low PPFD. The model calculations suggest the $H < 0$ in the energy balance is an outcome of evaporative cooling and low R_n. At higher PPFD, increases in H (i.e., $H > 0$; surface heating) occur due to rapid increases in $g_{b,H}$ with increasing U. This increase in H is mediated by the fact that the difference between T_s and T_a (i.e. the driving force for H) tends to diminish with increasing U (see Eq. (8)). Notwithstanding this compensatory effect arising from a reduced driving force for H, the overall increase in H results in a decrease in LE. This highlights the main mechanism leading to an apparent decline in f_e with increasing U. It may be stated that when $H < 0$, $\partial f_e/\partial U > 0$ for all U. However, when $H > 0$, $\partial f_e/\partial U < 0$ with further increases in U.

Similar to f_e, modeled f_c declines at high PPFD but increases at low PPFD with increasing U. The transition occurs when PPFD ≈ 1250 μ mol m^{-2} s^{-1} (i.e., lower than f_e). The increasing trend in f_c with increasing U at a low PPFD was also reported elsewhere [40] for tomato seedlings in a wind-tunnel type chamber. Different from f_e and f_c, a monotonic increase in g_{s,CO_2} with increasing U was maintained across all PPFD in the model calculations. Adopting well-coupled assumption, however, common models assume g_{s,CO_2} only serves as an upper limit for g_{t,CO_2} and remains constant for different U even when the leaf is 'decoupled' from the atmosphere at low wind speed (see Appendix C). The modeled g_{b,CO_2} here is dominated by forced convection (i.e., free convection is negligible) and $g_{b,CO_2} \gg g_{s,CO_2}$ (not shown here), leading to $g_{t,CO_2} \approx g_{s,CO_2}$ and $c_s \approx c_a$. These results illustrate how variations in g_{s,CO_2} can be associated with changing U even for well-coupled conditions between leaf and atmosphere. For a given U (i.e., the replenishment rate of CO_2 through the laminar boundary layer is fixed), larger c_i/c_s in the lower PPFD regime can be attributed to smaller assimilation rate so that c_i tends to be closer to c_s (i.e., the depletion rate of CO_2 in the stomatal cavity is low). On the other hand, increasing c_i/c_s with increasing U at a given PPFD suggests that g_{s,CO_2} promoted by g_{b,CO_2} at higher U resulted in larger replenishment rate of CO_2 in the stomatal cavity. Larger flux-based WUE ($= f_c/f_e$) was computed under low U and low PPFD due to faster reductions in

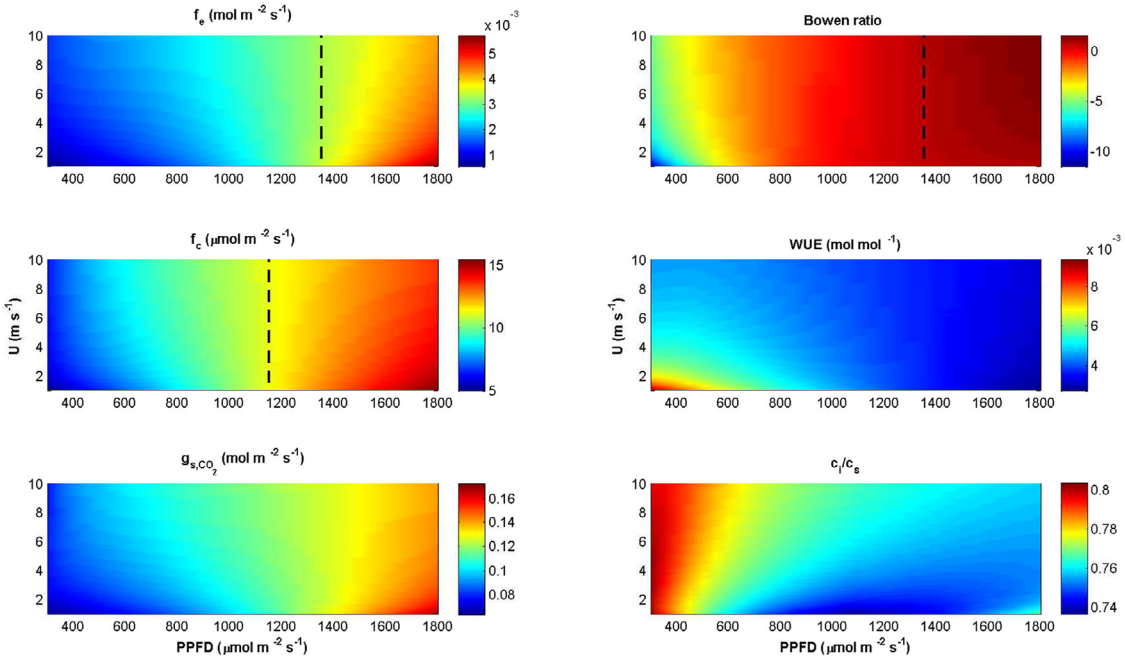

Fig. 4. The same as Fig. 3 but for water-stressed soil conditions ($\lambda = 5$ μ mol mol^{-1} kPa^{-1}) and small evaporative demand ($RH = 60\%$). Note that the transition PPFD for the reversal sign of $\partial f_e/\partial U$ and $\partial f_c/\partial U$ are 1350 and 1150 μ mol m^{-2} s^{-1} and represented by the broken lines, respectively. The broken line for Bowen ratio (≈0.75) represents the corresponding transition for f_e.

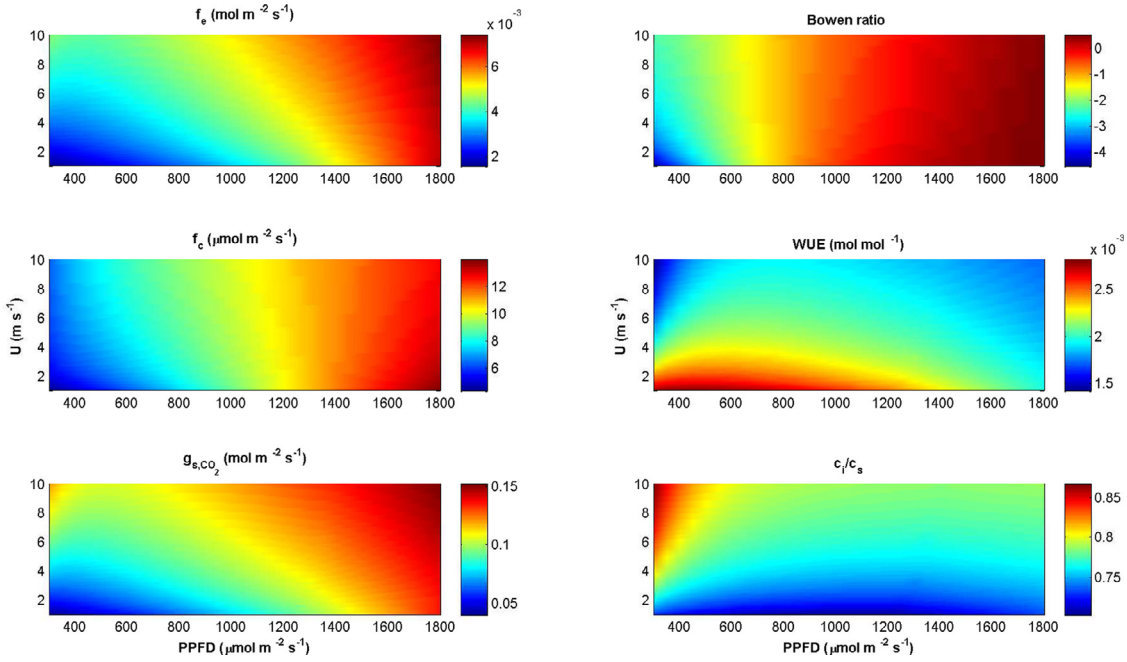

Fig. 5. The same as Fig. 3 but for well-watered soil condition ($\lambda = 0.001$ μ mol mol^{-1} kPa^{-1}) and high evaporative demand ($RH = 20\%$).

f_e with decreasing U when compared to f_c at low PPFD. This implies that WUE may be larger for leaves within the lower part of a canopy if the physiological, radiative, and aerodynamic characteristics are unaltered (though a less likely scenario given variations in leaf nitrogen content).

3.1.2. Water-stressed condition with small evaporative demand

Fig. 4 shows trends in f_e, f_c and g_{s,CO_2} with increasing U for variable PPFD when soil moisture is limiting (i.e., large λ). Modeled f_e and f_c trends with increasing U agree with their well-watered counterparts but their transitions are now 'shifted' to smaller PPFD (≈1350 and 1150 μ mol m^{-2} s^{-1} for f_e and f_c, respectively). The transition for f_e at a smaller PPFD can be explained again by the larger Bowen ratio due to the smaller f_e induced by water-stressed conditions (higher λ). Compared with well-watered conditions (see Fig. 3), g_{s,CO_2} is generally smaller. Also, g_{s,CO_2} does not significantly increase with increasing U in low PPFD and even decreases with increasing U in the high PPFD range. Field experiments [10] on two grapevine cultivars measured by porometry reported a reduced g_{s,CO_2} with increasing U, a pattern consistent with the model results here. Moreover, smaller c_i/c_s corresponding to a larger λ have been predicted for this scenario, which is supported by experiments and other model predictions

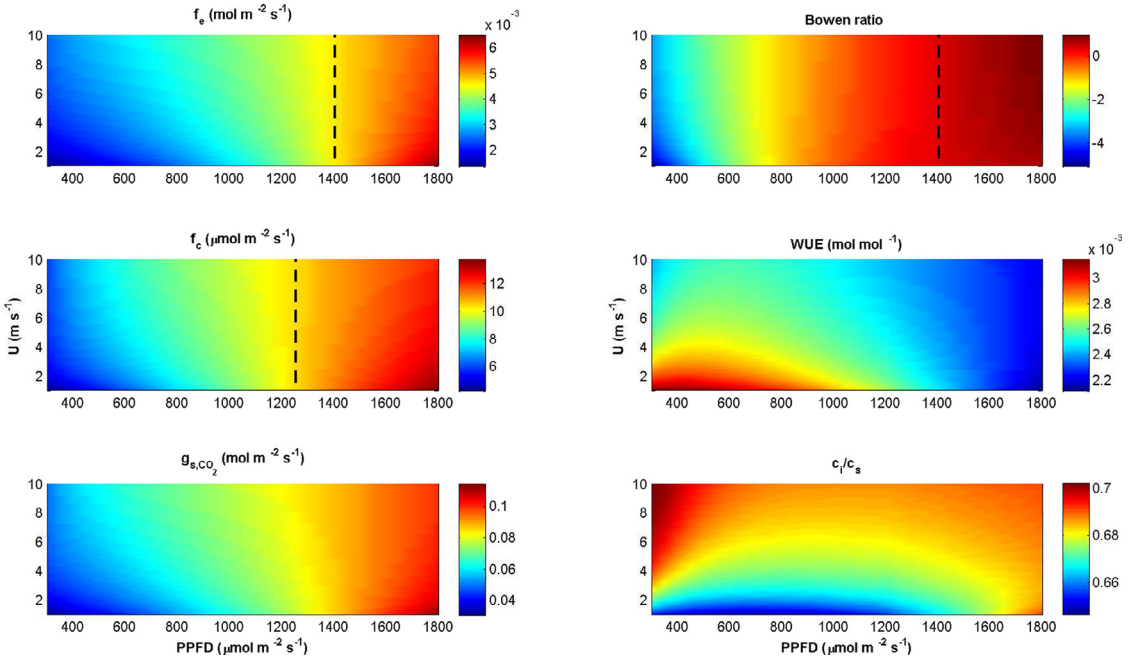

Fig. 6. The same as Fig. 3 but for water-stressed soil conditions ($\lambda = 5$ μ mol mol^{-1} kPa^{-1}) and high evaporative demand ($RH = 20$ %). Note that the transition PPFD for the reversal sign of $\partial f_e/\partial U$ and $\partial f_c/\partial U$ are 1400 and 1250 μ mol m^{-2} s^{-1} and represented by the broken lines, respectively. The broken line for Bowen ratio (≈0.75) represents the corresponding transition for f_e.

[37,55]. In general, c_i/c_s varies with g_{s,CO_2} ($\approx g_{t,CO_2}$) but its dependence on T_s in the physiological parameters of Eq. (6) complicates its variations with U. Thus, modeled c_i/c_s at the two end members of the light regime (i.e., very low and very high light PPFD) can exhibit non-monotonic variation with increasing U. As a consequence, the model results predict enhanced WUE compared to well-watered conditions because f_e is reduced more rapidly with increasing λ than f_c. Recall that f_c is impacted by another compensatory physiological mechanism (regulating c_i) and optimality conditions tend to maximize f_c for a given f_e. With progressively drying conditions in the soil, similar trends in WUE have been reported elsewhere again lending some support to the model results here [16,45,50]. This analysis suggests that WUE may increase with some reductions in water supply from the soil volume without significant reductions in plant photosynthesis (and possibly crop yield in some instances).

3.1.3. Large evaporative demand under well-watered conditions

The responses of f_e, f_c and g_{s,CO_2} to smaller *RH* (i.e., overall 'actual' evaporative demand is larger) under well-watered soil condition are shown in Fig. 5. When soil water availability is not limiting leaf transpiration, the effect of enhanced driving force from the atmosphere reduces g_{s,CO_2} monotonically (i.e., $\partial g_{s,CO_2}/\partial \mathrm{VPD} < 0$ for all VPD; roughly, $g_{s,CO_2} \sim \mathrm{VPD}^{-1/2}$ to a leading order; see [36]). This finding is consistent with Helox experiments (i.e., helium:oxygen mixture is used as a surrogate to control the 'actual' evaporative demand) reported elsewhere [53] and forms the basis of the Hamiltonian H_a. However, reduced g_{s,CO_2} due to larger evaporative demand diminishes f_c and c_i/c_s, but f_e is enhanced by increased evaporative demand because of the increased driving force (i.e., $f_e \sim \mathrm{VPD}^{-1/2} \times \mathrm{VPD}$ to a leading order). As a result, a decreasing overall WUE with larger evaporative demand emerges. Using leaf gas exchange measurements, the response of f_c and f_e as well as WUE to increasing evaporative demand for *Gossypium hirsutum* L. under well-watered condition, explored in glasshouse bays by [18], are consistent with the model calculations here. Since f_e increases with increasing evaporative demand, the H and Bowen ratio governed by the energy balance are subsequently reduced, leading to a shift in the transition PPFD where $\partial f_e/\partial U$ reverses sign with increasing U in a PPFD value well outside the range considered here. For the particular conditions explored here, $\partial f_e/\partial U > 0$ prevails for all PPFD commonly encountered in ecosystem studies. Evaporative cooling dominates throughout given that surface heating is reduced with increasing U even in high PPFD.

3.1.4. Large evaporative demand under water-stressed conditions

Fig. 6 shows the trends in f_e, f_c and g_{s,CO_2} with respect to variable U and PPFD when evaporative demand and soil water availability are simultaneously limiting leaf-level gas exchange with the atmosphere. Compared to the well-watered conditions with large evaporative demand (see Fig. 5), a further reduction in g_{s,CO_2} is expected due to limited soil water availability (i.e., larger λ). As discussed earlier, the overall decreasing trend in f_e, f_c and c_i/c_s can be simply explained by this reduced g_{s,CO_2}, given a constant driving force from the atmosphere. Similar to the comparison for small evaporative demand between the two end members of the soil water availability conditions (see Sections 3.1.1 and 3.1.2), the more rapid reduction of f_e than f_c results in enhanced WUE. Interestingly, the transition PPFD responsible for the reversed sign of $\partial f_e/\partial U$ emerges again. This is because the corresponding H and Bowen ratio are enhanced with decreasing LE (i.e., f_e) thereby shifting back the transition within the range of PPFD considered here. This transition occurs at PPFD ≈ 1400 μ mol m^{-2} s^{-1}.

To sum up, $\partial f_e/\partial U > 0$ is generally satisfied for low PPFD. However, $\partial f_e/\partial U$ at high PPFD can be positive or negative depending on the driving forces for transpiration (e.g., evaporative demand) and soil water availability (e.g., leaf water status and λ). Fig. 7 summarizes $\partial f_e/\partial U$ for a wide range of U and typical low and high PPFD, low and high evaporative demand and for two extreme λs representing different soil water availability. It is to be noted that when replacing the optimal stomatal conductance closure with BB or LEU formulations, qualitatively similar results emerge though the transition points shift to smaller PPFD due to the larger predicted values of f_e as shown in Appendix D.

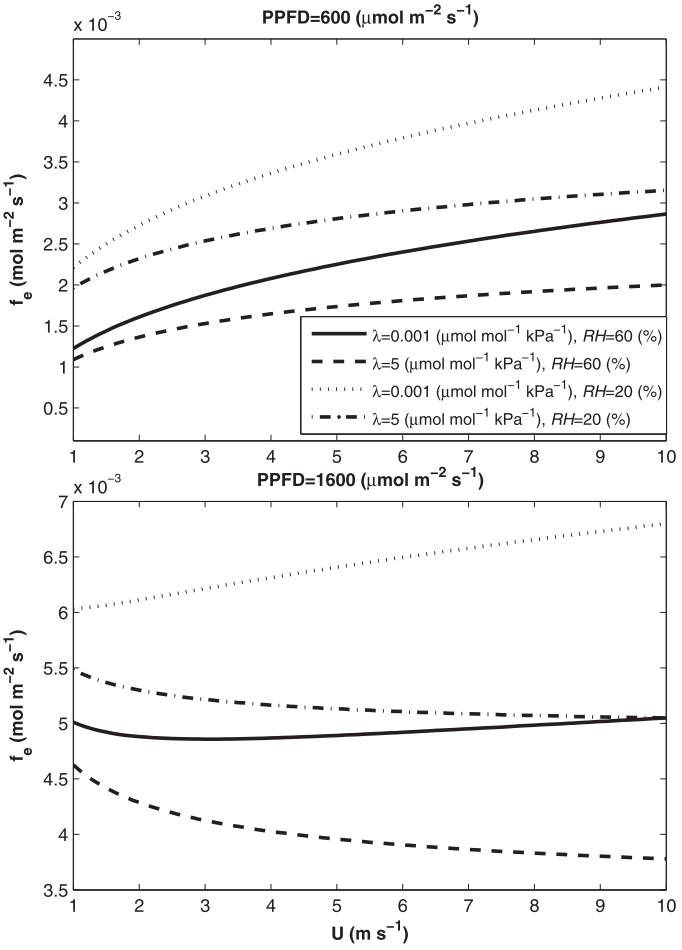

Fig. 7. The f_e–U trends under two selected light conditions (i.e., PPFD=600 and 1600 μ mol m^{-2} s^{-1}) for the four scenarios. Note that the model results here are extracted from Figs. 3–6 to illustrate the persistent monotonic increases in f_e under low light condition but possible non-monotonic variations or decreasing trends in f_e at the high light level.

3.2. Sap flow measurements in a wind tunnel

To further explore the variations in $\partial f_e/\partial U$ with increasing U, sapflow velocity (V_s) data reported by [11] are complemented by recent experiments on the same species and in the same wind tunnel. The experimental setup, the species used, and the soil moisture conditions are reviewed in Appendix A (see also Fig. 8). In the experiments here, only whole plant (or branch) steady-state transpiration rate F_e derived from V_s is available for two species across various U for: nocturnal (or PPFD=0) and low PPFD (=250 μ mol m^{-2} s^{-1}) and for two soil moisture states (well-watered and water-stressed). Steady-state conditions were checked for each prescribed U by waiting until measured $dV_s/dt \approx 0$. A major advantage of the wind tunnel setup is that all the leaves experienced steady and uniform U and PPFD permitting direct f_e-trend comparison with leaf-level gas exchange model calculations under given conditions. For comparisons with the model results, the focus is on the behavior of $\partial f_e/\partial U$ variations. Hence, to facilitate this comparison, measured transpiration rates are normalized using the scaling relation:

$$\frac{F_e}{F_{emax}} = \frac{V_s A_s}{V_{smax} A_s} = \frac{f_e A_l}{f_{emax} A_l} = \frac{V_s}{V_{smax}} = \frac{f_e}{f_{emax}} \tag{12}$$

where A_s and A_l are respectively the sapwood and total leaf area, and F_{emax} and f_{emax} are F_e and f_e at maximum wind speed for each set of PPFD and soil moisture conditions. Likewise, the model results are normalized by their f_e at maximum wind speed for each PPFD and soil moisture conditions. This normalization is selected because U variations are to be studied while all other conditions are held constant. The normalization for the measurements is expected to be reasonable under steady state conditions as is the case here (see Appendix A) and for a linear relation between F_e and V_s, which was reported by Chu et al. [11]. Recall that a direct comparison between measured and modeled f_e (or F_e) cannot be conducted due to the lack of A_s and A_l measurements as well as leaf-gas exchange parameters. As shown later through model calculations, such normalized f_e may be sufficiently adequate to capture plant system responses to U variations, which is the main focus here. Three physiological parameters must be *a priori* specified before implementing the proposed model: $V_{cmax,\,25}$, $J_{max,\,25}$ and λ. For all runs, including runs employing the published data from [11] and the recent wind-tunnel experiments, the $V_{cmax,\,25}$ and $J_{max,\,25}$ were taken to be 50 and 100 μ mol m^{-2} s^{-1} (see Table 1). Though leaf-level gas exchange measurements were not available to infer directly these parameters, a sensitivity analysis showed that when using normalized-f_e (i.e. f_e normalized by its maximum coinciding with the highest U for model and measurements) for comparisons, modeled normalized-f_e was not sensitive to the precise choice of $V_{cmax,\,25}$ and $J_{max,\,25}$ (see Appendix E). The values of λ used for the two species under different soil water conditions are summarized in Table A.2. For well-watered conditions (i.e., when the cost of water in carbon units is small), λ = 0.001 μ mol mol^{-1} kPa^{-1} and is arbitrarily selected. The normalized f_e variations with U are again not sensitive to this choice of λ provided its value is sufficiently small and finite [36] for well-watered soil conditions. However, a larger value of λ is expected when soil water availability is limited as mentioned before (see Section 3.1). The λ for *Pachira macrocarpa* and *Messerschmidia argentea* under water-stressed conditions were determined by fitting modeled to measured normalized-f_e. The resulting λ are respectively 0.85 and 3.5 μ mol mol^{-1} kPa^{-1} for *P. macrocarpa* and *M. argentea*, which are within the range reported for approximately 50 species [47]. It was found that trends in normalized-f_e with variable U chiefly depend on λ and PPFD once the evaporative demand, c_a, PPDF, and air temperature are set. Based on these findings, the wind-tunnel comparison presented here only utilizes normalized-f_e with pre-specified $V_{cmax,\,25}$ and $J_{max,\,25}$ as the goal is to illustrate the low PPFD condition responsible for the positive sign of $\partial f_e/\partial U$. For the computation of $g_{b,\,i}$, d is assumed to be 0.015 m for both species and all cases. The trends in the measurements and models for normalized f_e are now presented for the published and the more recent wind tunnel experiments.

3.2.1. Previous wind-tunnel experiments [11]

Where possible, the measured nocturnal (i.e. PPDF=0) sap flow in the previous wind-tunnel experiments [11] are used for inferring g_{res} (see discussion in Section 2.1). It is inferred by matching normalized-f_e computed from the energy balance to the steady-state sap flow measurement (i.e., no capacitive effects and water refilling the xylem) for various U. Furthermore, this g_{res} is assumed to be independent of g_{s,H_2O} so that $\partial g_{res}/\partial g_{s,H_2O} = 0$ as noted earlier. Using published data reported elsewhere [11], the measured nocturnal f_e (i.e. at PPFD=0) normalized by the maximum nocturnal f_e (labeled as $fn_{e,\,max}$) at maximum U versus the modeled results with the best-fit g_{res} = 0.04 mol m^{-2} s^{-1} is shown in Fig. 9(a). The best-fit g_{res} was determined from a 'global search' that minimizes the root-mean squared percent error (*RMSPE*) between modeled and measured $f_e/fn_{e,\,max}$ during conditions where PPFD=0. Here, the *RMSPE* is defined as

$$RMSPE = \sqrt{\frac{1}{N}\sum_{i=1}^{N} \Delta_i^{\,2}} \times 100, \tag{13}$$

where N is the number of data points and Δ_i is the difference between measured and modeled $f_e/fn_{e,\,max}$ computed solely from energy balance considerations. During nighttime (i.e. PPFD=0), the

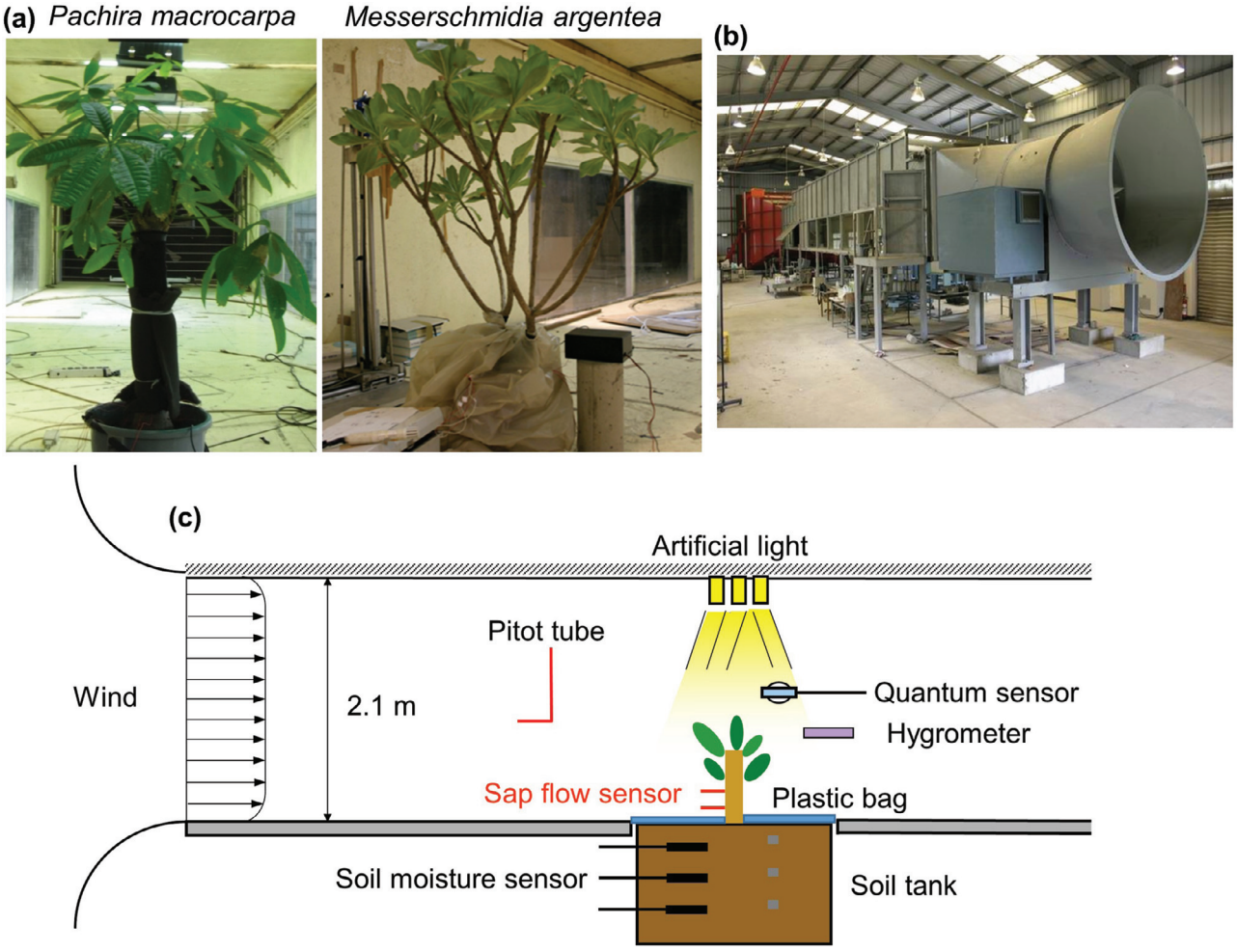

Fig. 8. (a) A photograph of the two broadleaf species, (b) the wind-tunnel and (c) schematic of the wind-tunnel setup.

main external driver responsible for f_e variability is variation in U (i.e., g_{b,H_2O}) given that the evaporative demand (i.e., T_a and RH) and g_{res} are constants and the soil was well-watered in those published experiments [11]. The constant g_{res} here does not imply a constant f_e when U increases, and in fact, nocturnal f_e does increase with increasing U through g_{b,H_2O}. It is to be noted that $g_{res} = 0.04$ mol m^{-2} s^{-1} is determined only from these prior experiments. The data set described in Appendix A are not used in the inference of g_{res} as the aforementioned data are all collected at PPFD=250 μ mol m^{-2} s^{-1} (i.e. no nocturnal like runs).

Inserting the best-fit g_{res} (= 0.04 mol m^{-2} s^{-1}) into the leaf-level gas exchange model described in Section 2, Fig. 9(b) shows reasonable agreement between measured and modeled daytime normalized-f_e reported in [11] for well-watered soil condition for different U at PPFD= 250 μ mol m^{-2} s^{-1}. The g_{res} only serves as an additional pathway for water vapor transport (but not CO_2) during daytime. As suggested elsewhere [8], no experimental evidence has been presented that shows significant impact of g_{res} on g_{s,CO_2} or carbon gain. Additionally, model sensitivity analysis (not shown here) was conducted on g_{res} demonstrating that g_{s,CO_2} and f_c are not sensitive to variations in g_{res}, which only provides a base line value for f_e during daytime conditions. The increasing trend in modeled g_{s,CO_2} (not g_{t,CO_2}) with increasing U is presented in Fig. 9(c) for the same conditions as those in Fig. 9(b). The monotonic increase in f_e and g_{s,CO_2} with increasing U occurs at low PPFD reported here, which is consistent with other wind-tunnel studies conducted at low PPFD regimes [23,25,31,49].

3.2.2. Recent wind-tunnel experiments

For the two species in the present wind-tunnel experiment, the comparison between measured and modeled daytime (i.e. PPFD = 250 μ mol m^{-2} s^{-1}) f_e normalized by the corresponding maximum daytime f_e under two different soil water conditions across a wide range of U is shown in Fig. 10. Previous data from [11] are included only for reference (see Fig. 9(b)). In Fig. 10, the arrow indicates the direction of increasing U. Similar to Fig. 9(b), the normalized-f_e for each species at a given soil water status monotonically increases with increasing U at the low PPFD that is consistent with model predictions. It should be noted again that we do not attempt to conduct a one-to-one comparison between measured and modeled absolute f_e given the absence of leaf physiological measurements, leaf area index, and leaf-to-sapwood area. Only trends in measured sap flow velocity at steady-state conditions, when properly normalized, are used for such qualitative comparisons between measured and modeled f_e with increasing U. To be clear, the recent experiments are employed as independent data sources to show only the increasing trends in f_e with increasing U at low PPFD for the two different species and two different soil water availability. Moreover, measured V_s (used as a surrogate to f_e) for the two species under water-stressed soil conditions was significantly smaller when compared to their well-watered counterparts. The reductions in V_{smax} are approximately 20% and 15% for *P. macrocarpa* and *M. argentea*, respectively. It is also suggested that the potted plants did sense soil moisture stress even though the drop in the measured water saturation is only 10% (see Table A.2) between well-watered and water-stressed conditions. To sum up, these

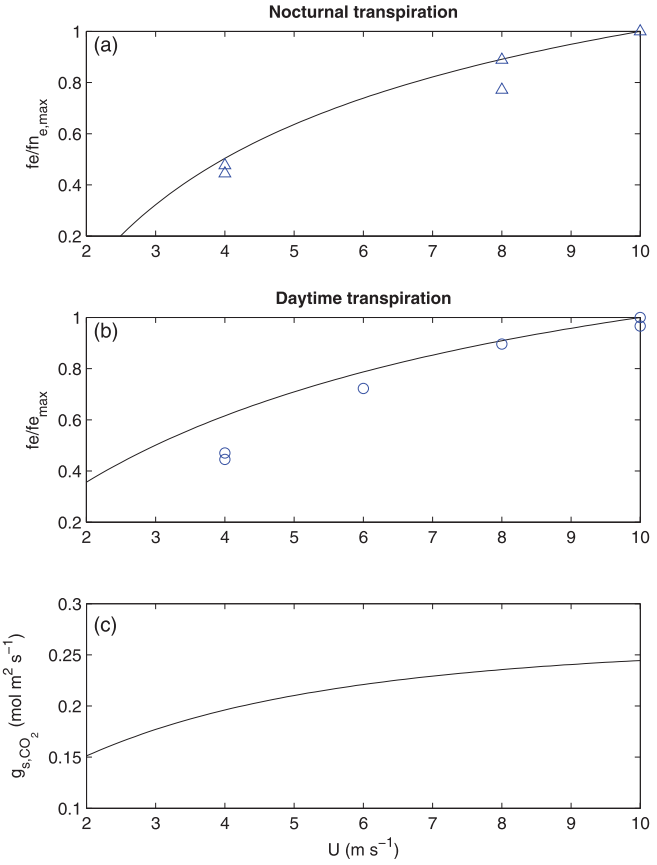

Fig. 9. (a) Comparisons between measured (symbols) and modeled (solid line) nocturnal f_e normalized by its maximum nocturnal value for different wind speed conditions(U). (b) The same as figure (a) but for daytime normalized-f_e, where the normalization is based on maximum daytime value. (c) Modeled stomatal conductance (g_{s,CO_2}) under different wind conditions. The data is taken from [11]. Note that the best-fit nocturnal residual conductance ($g_{res} \approx 0.04$ mol m^{-2} s^{-1}) is first obtained from matching nocturnal f_e computed through energy balance to the measured nocturnal f_e as shown in (a), and the optimality hypothesis is implemented to compute daytime f_e and g_{s,CO_2} as shown in (b) and (c).

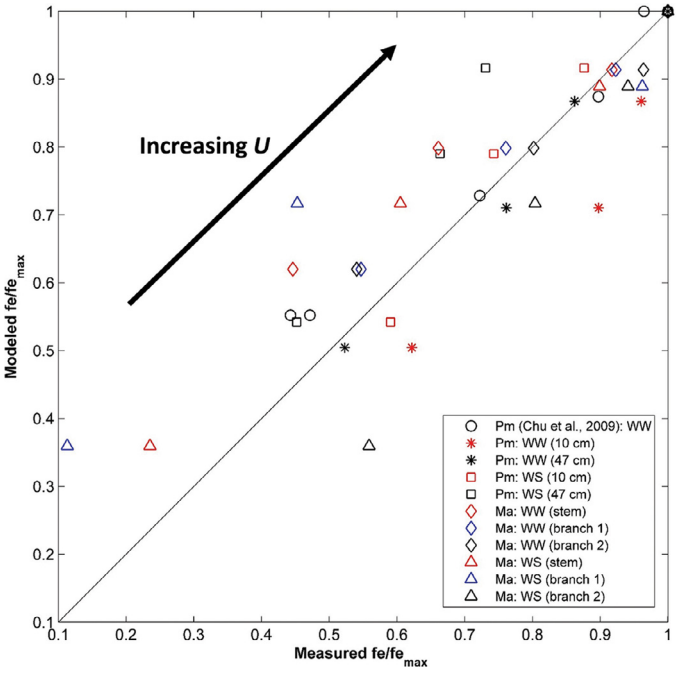

Fig. 10. Comparison between measured and modeled normalized-f_e during daytime for *Pachira macrocarpa* (Pm) and *Messerschmidia argentea* (Ma) for different soil water conditions and across a wide range of wind speeds. The solid line represents 1:1 line. The coefficient of determination $R^2 = 0.85$ ($p < 0.01$). Note that WW and WS respectively refer to well-watered and water-stressed condition. The direction of increasing U is also indicated by the arrow suggesting $\partial f_e/\partial U > 0$ for all data set at low PPFD.

comparisons suggest that the proposed model reasonably recovers the patterns reported in the wind tunnel experiment for steady low PPFD and quasi-steady soil moisture states and across a wide range of wind speeds.

3.3. Study limitation

Given all the assumptions made to arrive at the model and the f_e-trend comparison between modeled and measured results, it is instructive to recapitulate the limitations of the leaf-level gas exchange model and the wind tunnel experiments. Regarding the model development, the premise is $U > 0$ that guarantees a finite $g_{b,i}$ (i.e., g_{t,CO_2} and g_{t,H_2O}). Without considering all the details of the biochemical signaling that govern movement of guard cells and mechanical constraints on this movement, the closure for g_{s,CO_2} is based on an assumption that stomates operate optimally to maximize carbon gain per unit water loss. This assumption, while generally accepted and supported by a large corpus of data, needs not hold when limitations other than water availability exist. Also, the calculations for $g_{b,i}$ rely on empirical formations and an effective leaf dimension (i.e., d) that needs further elaboration to account for detailed aerodynamic modifications surrounding leaf bodies due to wind contact angle, leaf orientation and micro-roughness of the leaf surface. The energy balance assumes leaves have no thermal inertia and that surface temperature adjusts instantly to changes in wind speed. For some species, this assumption appears to be fair [38] though leaf thermal properties and leaf volume must be factored in. Last, the calculations here ignore the mesophyll conductance that may become limiting under increased soil moisture stress conditions.

Direct comparisons between modeled and measured f_e in the wind tunnel was not possible as well. The lack of measured physiological parameters and the absence of total leaf area needed to convert sapflow velocity to transpiration rate for the potted plants was the main cause for the absence of such one-to-one comparison. Another major limitation of the wind tunnel experiment is the lack of high PPFD conditions, especially at PPFD values where the f_e-U reversed its monotonically increasing trend. Notwithstanding all the aforementioned issues, the overall trends in actual f_e with respect to U are reflected in measured steady-state V_s through the normalization when all other conditions (i.e., PPFD, A_l, A_s and soil water status) are maintained nearly constant throughout each experiment.

4. Conclusion

The primary goal here was to explain the conditions leading to $\partial f_e/\partial U > 0$ or < 0 with increasing U. To address this goal, the sign of $\partial f_e/\partial U$ was mainly discussed with the aid of a gas transfer model that explicitly accounts for boundary layer conductance, evaporative cooling, and soil moisture stress across a wide range of wind speed conditions. The model combines the Farquhar photosynthesis model for atmospheric CO_2 demand with stomatal optimization theories to infer f_e. Consistent with model prediction, a positive sign of $\partial f_e/\partial U$ at low PPFD regime was shown by published and newly reported sap flow measurements conducted in a wind tunnel for two species (i.e., *P. macrocarpa* and *M. argentea*) across a wide range of wind speed and two different soil water availability. Based on model results for a broad range of environmental conditions and wind tunnel measurements for a restricted range of environmental conditions, a number of conclusions can be drawn:

(1) Leaf-level transpiration monotonically increases with increasing mean wind speed when PPFD is low. This finding is supported by both sap flow measurements in the wind-tunnel and model calculations. However, the model calculations also suggest a possible $\partial f_e/\partial U < 0$ at high PPDF levels. This transition from $\partial f_e/\partial U > 0$ to $\partial f_e/\partial U < 0$ occurs when the Bowen ratio is ≥ 0.75. To be specific, surface cooling (i.e., $H < 0$) at low light regime guarantees a $\partial f_e/\partial U > 0$ for all U. At high light levels, $\partial f_e/\partial U < 0$ can occur due to surface heating (i.e., $H > 0$) that suppresses f_e because of rapid increases in H with increasing U if net radiation at the leaf surface remains roughly the same.

(2) When soil water availability is limited, the transition PPFD value reflecting the reversed sign of $\partial f_e/\partial U$ tends to be lower. This can be explained by reduction in f_e (i.e., evaporative cooling) that enhances H (i.e., surface heating) and Bowen ratio leading to a transition at a lower light regime. On the other hand, $\partial f_e/\partial U < 0$ may not be realized for common environmental conditions when atmospheric evaporative demand is large under well-watered soil condition. Given this specific condition, evaporative cooling dominates and $\partial f_e/\partial U > 0$ prevails for all PPFD.

(3) Modeled stomatal conductance to CO_2 (i.e., g_{s,CO_2}) can be impacted positively or negatively by aerodynamic modifications based on U, especially when the leaf is 'decoupled' from the atmosphere. The assimilation and transpiration rates as well as the ratio of the inter-cellular to ambient atmospheric CO_2 concentration and WUE are also altered by wind speed conditions. The degree of alteration depends on environmental factors (e.g., light availability, water availability in the soil and evaporative demand) imposed upon the plant system. Unlike models that assume well-coupled conditions, the proposed modeling approach is capable of capturing theses non-monotonic behaviors with respect to U. Thus, it may be used to improve the predictability of canopy-level CO_2 and H_2O fluxes reflecting whole-plant responses to the environment. As U and PPFD can be highly variable within vegetated canopies, the model up-scaling process from leaf to canopy level requires appropriate coupling to the light attenuation and flow field (e.g., [43]) given information on leaf area density and leaf nitrogen content distributions.

Current uncertainties in modeling leaf-level gas exchange for CO_2 and water vapor can be reduced when the interplay between the micro-environment (i.e., flow and temperature fields) and leaf attributes (e.g., d) are appropriately described without implementing empirical formulations to determine the boundary layer conductances. Moreover, the model calculations are only valid for finite U. Given that finite U throughout vegetated medium is not uncommon in many ecosystems [35] suggests that this limitation may not be too restrictive for natural settings. Future studies on the measurements of g_{s,CO_2}, f_e and f_c within the laminar boundary layer when leaves experience natural U are needed to evaluate the proposed model predictive ability. Also, additional laboratory and field experiments for different species are required to differentiate wind effects on transpiration rate at the leaf scale from canopy scales, especially when the vertical distributions of leaf orientation, radiative forcing and wind speed within tall canopies are statistically non-uniform.

Acknowledgments

Support from the National Science Foundation (NSF-CBET-103347 and NSF-EAR-1344703), the U.S. Department of Energy (DOE) through the Office of Biological and Environmental Research (BER) Terrestrial Carbon Processes (TCP) program (DE-SC0006967 and DE-SC0011461), the Nicholas School of the Environment at Duke university Seed Grant Initiative, and the Swedish Research Council FORMAS through a project: Nitrogen and Carbon in Forests is acknowledged.

Appendix A. Experiment

The effects of variable U on f_e were explored using sap flow measurements for two potted broadleaf species (i.e., *P. macrocarpa* and *M. argentea*) placed in a large wind-tunnel (see Fig. 8). The working section of the wind tunnel is 18.5 m long, 2.1 m tall and 3.0 m wide as described in [11]. Sap flow measurements were conducted across a wide range of U (up to 8 m s^{-1}) at a fixed PPFD (=250 μ mol m^{-2} s^{-1} for all runs) or zero PPFD (plants covered). The soil type in the pot was sandy loam with a permanent wilting point (on a volume basis) of $\theta_w = 5.6\%$. Two scenarios were explored for soil water availability: (1) well-watered and (2) water-stressed conditions. For well-watered conditions, the soil was watered with plethoric water and drainage through a small hole at the bottom of the pot proceeded for three hours prior to each experiment. For water-stressed conditions, the pot was not watered for 12 days and volumetric soil moisture θ measured by a soil moisture sensor (EC10, Decagon Inc.) positioned at 5.0 cm underneath the soil surface dropped from $\theta = 35.8\%$ for near saturated conditions to $\theta = 27.7\%$ and $\theta = 24.0\%$ for *Pachira macrocarpa* and *Messerschmidia argentea*, respectively.

Table A.1
Characteristics of the stem and the branches.

Species		*Pachira macrocarpa*	*Messerschmidia argentea*
Total height (cm)		130	130
Main stem height (cm)		72	10
Main stem diameter (cm)		5.6	5.34
Branch 1	Diameter (cm)	–	3.45
	Length (cm)	–	12
Branch 2	Diameter (cm)	–	2.44
	Length (cm)	–	26

In this open-circuit suction-type wind-tunnel, the plant pot was placed in a soil tank covered with plastic bag to prevent soil evaporation in the test section. For both well-watered and water-stressed soil condition, $U = 2$, 4, 6 and 8 m s^{-1} in the test section were produced by a fan and monitored by a pitot tube. Granier-type [26] heat dissipation sensors were employed for measuring sap flow and their calibration as well as installation details are described in [11]. During the course of each experiment, any potential cooling effect induced by increasing U were minimized by covering the sensors with Styrofoam. Sap flow velocities (V_s) were measured simultaneously at two different locations (i.e., 10 cm and 37 cm from the soil surface) along the main stem for *Pachira macrocarpa*. V_s was measured in the main stem and two branches for *Messerschmidia argentea*. The stem and branch characteristics for each species are presented in Table A.1.

Table A.2
Environmental factors and the marginal water use efficiency for the two species under two soil water conditions.

Species	*Pachira macrocarpa*		*Messerschmidia argentea*	
Soil water condition	Well-watered	Water-stressed	Well-watered	Water-stressed
Volumetric soil moisture θ (%)	35.8	27.7	35.8	24.0
Air temperature T_a (°C)	31.4	24.4	22.0	16.3
Relative humidity RH (%)	56.4	89.3	90.3	93.5
Photosynthetically active radiation PPFD (μ mol m^{-2} s^{-1})	250	250	250	250
Marginal water use efficiency[a] λ (μ mol mol^{-1} kPa^{-1})	0.000035	0.85	0.000035	3.5

[a] The λ values were assumed to be small and finite for well-watered soil condition [36], but larger for dryer soil [37,46,47].

Steady-state U can be achieved approximately one to two minutes after the fan was turned on or when U was altered. Following any abrupt alteration to U, a transient duration of 20–50 min is required for V_s to reach a new steady state condition [11]. The data reported here are all collected when V_s attains steady state at each U. Environmental factors such as PPFD, T_a and RH were measured during the course of each experiment and remained nearly unaltered at the ambient indoor conditions. T_a and RH were respectively measured to a resolution of $\pm$ 0.1 °C and $\pm$ 2% using a hygrotransmitter (HD9008TR, Delta Ohm Inc.). PPFD was nearly constant and controlled by multiple lamps and monitored by a quantum sensor (LI-190SZ, LI-COR Inc.). All instrument signals were recorded by a data logger (CR10X, Campbell Scientific Inc.) throughout each experiment. The average values of the environmental factors for these two species are summarized in Table A.2.

Appendix B. List of symbols

All the symbols and units used throughout are summarized in Table B.1.

Table B.1
Nomenclature.

Symbol	Description	Unit
A_s	Sapwood area	m^2
A_l	Total leaf area	m^2
C_{oa}	Ambient oxygen concentration	mmol mol^{-1}
H	Sensible heat flux	W m^{-2}
J	Electron transport rate	μ mol m^{-2} s^{-1}
J_{max}	Light saturated rate of electron transport	μ mol m^{-2} s^{-1}
$J_{max,\,25}$	Normalized J_{max} at 25 °C	μ mol m^{-2} s^{-1}
K_c	Michaelis constants for CO_2 fixation	μ mol mol^{-1}
K_o	Michaelis constants for oxygen inhibition	mmol mol^{-1}
L	Latent heat of water vaporization	J mol^{-1}
LE	Latent heat flux	W m^{-2}
PPFD	Photosynthetically active radiation	μ mol m^{-2} s^{-1}
P_a	Atmospheric pressure	kPa
Q_n	Net radiation	W m^{-2}
Q_{abs}	Absorbed radiation	W m^{-2}
Q_{out}	Emitted longwave radiation	W m^{-2}
R_d	Daytime mitochondrial respiration rate	μ mol m^{-2} s^{-1}
RH	Relative humidity	%
T_a	Leaf surface temperature	°C
T_i	Intercellular temperature	°C
T_s	Ambient temperature	°C
U	Mean wind speed	m s^{-1}
VPD	Vapor pressure deficit	kPa
$V_{c,\,max}$	Maximum carboxylation capacity under light-saturated conditions	μ mol m^{-2} s^{-1}
$V_{cmax,\,25}$	Normalized $V_{c,\,max}$ at 25 °C	μ mol m^{-2} s^{-1}
WUE	Water use efficiency	mol mol^{-1}
c_a	Ambient CO_2 concentration	μ mol mol^{-1}
c_i	Intercellular CO_2 concentration	μ mol mol^{-1}
c_p	Capacity of dry air at constant pressure	J mol^{-1} K^{-1}
d	Characteristic dimension of the leaf	m
e_a	Ambient water vapor pressure	kPa
$e_a^*(T_a)$	Saturated water vapor pressure at a given T_a	kPa
e_i	Inter-cellular water vapor pressure	kPa
f_c	Assimilation rate	μ mol m^{-2} s^{-1}
f_e	Transpiration rate	mol m^{-2} s^{-1}
g_{b,CO_2}	Laminar boundary layer conductance for CO_2	mol m^{-2} s^{-1}
g_{b,H_2O}	Laminar boundary layer conductance for water vapor	mol m^{-2} s^{-1}
$g_{b,\,H}$	Laminar boundary layer conductance for heat	mol m^{-2} s^{-1}
g_{cut}	Cuticular conductance to water vapor	mol m^{-2} s^{-1}
g_{night}	Nighttime stomatal conductance to water vapor	mol m^{-2} s^{-1}
g_{res}	Nocturnal residual conductance	mol m^{-2} s^{-1}
g_{s,CO_2}	Stomatal conductance to CO_2	mol m^{-2} s^{-1}
g_{s,H_2O}	Stomatal conductance to water vapor	mol m^{-2} s^{-1}
g_{t,CO_2}	Total conductance for CO_2	mol m^{-2} s^{-1}

(continued on next page)

Table B.1 (*continued*)

Symbol	Description	Unit
g_{t,H_2O}	Total conductance for water vapor	mol m^{-2} s^{-1}
Γ^*	CO_2 compensation point	μ mol mol^{-1}
ϵ_s	Leaf surface emissivity	Dimensionless
σ	Stefan-Boltzmann constant	W m^{-2} K^{-4}
λ	Marginal water use efficiency	μ mol mol^{-1} kPa^{-1}
θ	Volumetric soil moisture (on a volume basis)	%
θ_w	Permanent wilting point (on a volume basis)	%

Appendix C. Leaf gas exchange model with well-coupled assumption

When interpreting leaf gas exchange measurements in cuvettes, well-coupled condition between the leaf and atmosphere (i.e., $g_{b,\,i} \gg g_{s,\,i}$) is commonly assumed and the mass transfer of CO_2 and water vapor adjacent to the leaf surface are given by:

$$f_c = g_{s,CO_2}(c_a - c_i)$$
$$f_e = a g_{s,CO_2}\mathrm{VPD}, \tag{C.1}$$

where $a = 1.6$ is the relative diffusivity of water vapor with respect to CO_2. Eq. (C.1) also implies that $T_s \approx T_a$, $c_s \approx c_a$ and $e_i - e_a \approx$VPD.

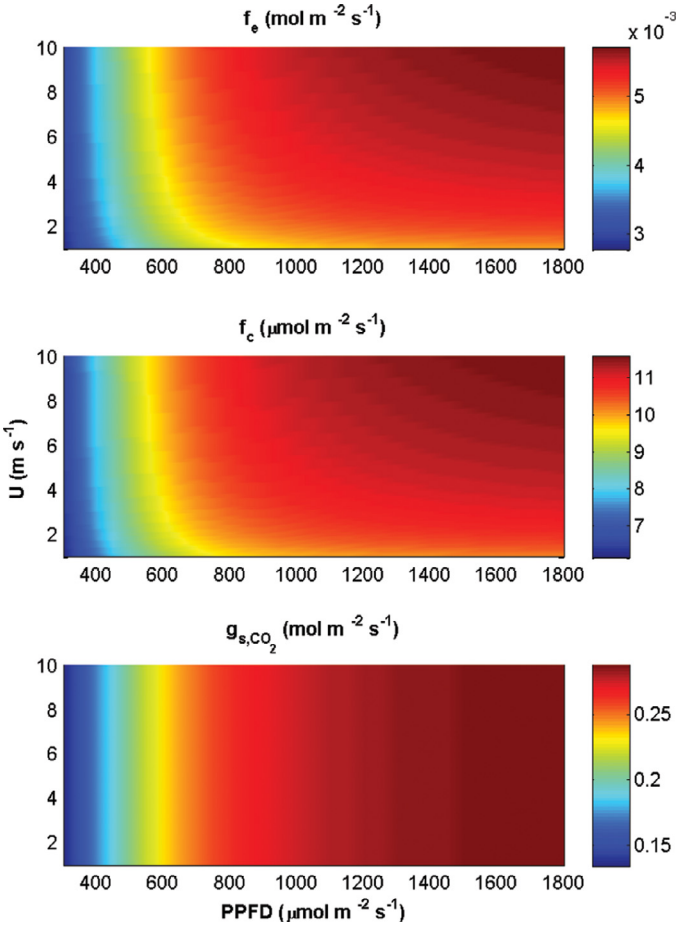

Fig. C.1. Modeled f_e, f_c and g_{s,CO_2} as a function of U and PPFD for well-watered soil condition ($\lambda = 0.001$ μ mol mol^{-1} kPa^{-1}) and small evaporative demand ($RH = 60\%$).

Combining Eqs. (C.1) and (5), c_i and f_c can now be expressed as a function of g_{s,CO_2} instead of g_{t,CO_2}:

$$\frac{c_i}{c_a} = \frac{1}{2} + \frac{1}{2g_{s,CO_2}c_a}[-k_1 - k_2 g_{s,CO_2} + R_d + \sqrt{\left[k_1 + (k_2 - c_a)g_{s,CO_2} - R_d\right]^2 - 4g_{s,CO_2}\left(-c_a g_{s,CO_2}k_2 - k_2 R_d - k_1\Gamma^*\right)}] \quad (C.2)$$

and

$$f_c = \frac{1}{2}[k_1 + (k_2 + c_a)g_{s,CO_2} + R_d - \sqrt{\left[k_1 + (k_2 - c_a)g_{s,CO_2} - R_d\right]^2 - 4g_{s,CO_2}\left(-c_a g_{s,CO_2}k_2 - k_2 R_d - k_1\Gamma^*\right)}]. \quad (C.3)$$

When optimality hypothesis (see Section 2.5) is again employed as a closure for g_{s,CO_2}, an analytical form of g_{s,CO_2} can be derived:

$$g_{s,CO_2} = \frac{-(c_a(k_1 - R_d) - k_2(k_1 + R_d) - 2k_1\Gamma^*)(a\mathrm{VPD}\lambda)}{(c_a + k_2)^2(c_a + k_2 - a\mathrm{VPD}\lambda)} + \frac{\sqrt{a\mathrm{VPD}\lambda k_1(k_2 + \Gamma^*)(k_2 R_d + ca(-k_1 + R_d) + k_1\Gamma^*)(c_a + k_2 - 2a\mathrm{VPD}\lambda)^2(-c_a - k_2 + a\mathrm{VPD}\lambda)}}{a\mathrm{VPD}\lambda(c_a + k_2)^2(c_a + k_2 - a\mathrm{VPD}\lambda)}. \quad (C.4)$$

It is evident that the predicted g_{s,CO_2} is not impacted by U at a given PPFD when the well-coupled approximation is adopted. However, previous models often combine this representation of g_{s,CO_2} with boundary layer conductance to accommodate wind effects on f_e and f_c, leading to monotonic increases in f_e and f_c with increasing U. To contrast, the modeled f_e, f_c and g_{s,CO_2} with respect to variable U and PPFD for well-watered soil condition ($\lambda = 0.001$ μ mol mol^{-1} kPa^{-1}) and small evaporative demand ($RH = 60\%$) (the same conditions as Section 3.1.1) are shown in Fig. C.1. The predicted f_e and f_c can deviate from the modeled results without invoking the well-coupled approximation (see Fig. 3) by up to 60% and 17% at high wind speed conditions, which is not trivial.

Appendix D. Ball-Berry and Leuning semi-empirical models

Two formulations of g_{s,CO_2} – the Ball-Berry (BB) [3] and the Leuning models (LEU) [44] – are commonly adopted in climate [56,57]

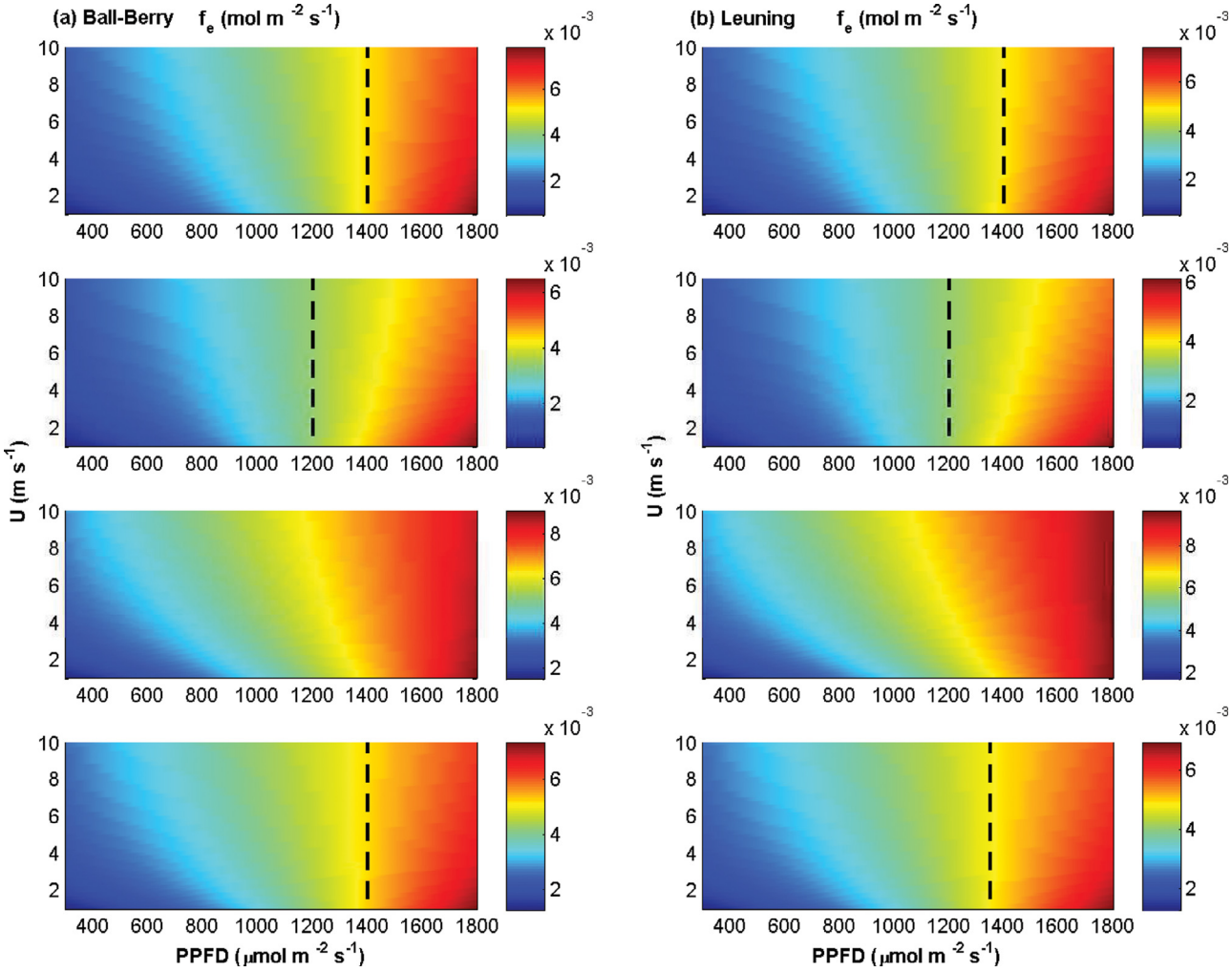

Fig. D.1. Modeled f_e using (a) Ball-Berry and (b) Leuning models assuming the same conditions for the four scenarios discussed in Section 3.1. Well-watered soil conditions with small evaporative demand, water-stressed soil conditions with small evaporative demand, large evaporative demand under well-watered soil moisture conditions and large evaporative demand under water-stressed soil moisture conditions are respectively shown from top to bottom panels. Note that the transition PPFD for the sign reversal of $\partial f_e/\partial U$ is represented by broken lines.

or biosphere-atmosphere [2,33,42,58] gas exchange models. They are represented as:

$$g_{s,CO_2} = m\frac{f_c}{c_a - \Gamma^*}F \tag{D.1}$$

where ms (i.e., respectively denoted as m_{BB} and m_{LEU} for BB and LEU) are the empirical fitting parameters and the reduction functions Fs are respectively $F_{BB} = RH$ and $F_{LEU} = (1 + \mathrm{VPD}/D_0)^{-1}$ where D_0 is a normalizing constant for BB and LEU.

The BB and LEU models are employed as alternatives to close the system of equations discussed in Section 2 instead of the optimality hypothesis so as to further assess whether a non-monotonic $f_e - U$ relation is robust to such optimality condition. To illustrate, it is assumed that $\Gamma^* = 50$ μ mol mol^{-1}, $D_0 = 3$ kPa and the same conditions for the four scenarios discussed in Section 3.1. The empirical parameters ms are estimated by setting $m_{BB} = [RH(1 - c_i/c_a)]^{-1}$ and $m_{LEU} = (1 + \mathrm{VPD}/D_0)(1 - \Gamma^*/c_a)(1 - c_i/c_a)^{-1}$ [34]. The computed c_i/c_s from the optimality model under high PPFD and high wind conditions (approximating well coupled state) is adopted when determining the ms in BB and LEU so as to ensure their equivalence to optimality theory for such conditions. Next, the f_e as a function of U and PPFD computed by BB and LEU are shown in Fig. D.1. These results maintain similar patterns when compared to the optimality model for stomatal conductance (see Figs. 3–5) such as the transitions of the modeled f_e trends with increasing U. It is safe to state that the conclusions drawn from the modeling work here about the non-monotonic response of f_e to U is not sensitive to the precise stomatal closure approximation used to model the stomatal conductance. This completes the objective of the appendix.

Appendix E. Sensitivity analysis

A sensitivity index I is defined as:

$$I = \sqrt{\frac{1}{N}\sum_{i=1}^{N}(O - O_0)_i^2} \times 100 \tag{E.1}$$

where O_0 is the model output calculated from the pre-specified input variables (i.e., $V_{cmax,25} = 50$ μ mol m^{-2} s^{-1} and $J_{max,25} = 100$ μ mol m^{-2} s^{-1}), O is the model output calculated by altering input variables according to data reported elsewhere [61,62] and N is the number of data points. The index I is selected here to assess the sensitivity of the model output due to the model parameter variability. The uncertainties of the input variables for the proposed model are listed in Table E.1. Table E.1 shows that the uncertainties for the two physiological model parameters have minor impact on the model results (i.e., maximum I is small).

Table E.1
Sensitivity index I for the pre-specified input variables.

	$J_{max,25}$ (μ mol m^{-2} s^{-1})	$V_{cmax,25}$ (μ mol m^{-2} s^{-1})
Range	75–125	25–75
Maximum I (%)	3.12	1.33

References

[1] Baldocchi D, Falge E, Gu L, Olson R, Hollinger D, Running S, et al. Fluxnet: a new tool to study the temporal and spatial variability of ecosystem-scale carbon dioxide, water vapor, and energy flux densities. Bull Am Meteorol Soc 2001;82(11):2415–34. http://dx.doi.org/10.1175/1520-0477(2001)082⟨2415:FANTTS⟩2.3.CO;2.

[2] Baldocchi D, Meyers T. On using eco-physiological, micrometeorological and biogeochemical theory to evaluate carbon dioxide, water vapor and trace gas fluxes over vegetation: a perspective. Agric For Meteorol 1998;90(1):1–25. http://dx.doi.org/10.1016/S0168-1923(97)00072-5.

[3] Ball JT, Woodrow IE, Berry JA. A model predicting stomatal conductance and its contribution to the control of photosynthesis under different environmental conditions. In: Progress in photosynthesis research. Springer; 1987. p. 221–4. http://dx.doi.org/10.1007/978-94-017-0519-6_48.

[4] Bernacchi CJ, Singsaas EL, Pimentel C, Portis AR Jr, Long SP. Improved temperature response functions for models of rubiscoimited photosynthesis. Plant Cell Environ 2001;24(2):253–9. http://dx.doi.org/10.1111/j.1365-3040.2001.00668.x.

[5] Berninger F, Hari P. Optimal regulation of gas exchange: evidence from field data. Ann Bot 1993;71(2):135–40. http://dx.doi.org/10.1006/anbo.1993.1017.

[6] Betts R, Boucher O, Collins M, Cox P, Falloon P, Gedney N, et al. Projected increase in continental runoff due to plant responses to increasing carbon dioxide. Nature 2007;448(7157):1037–41. http://dx.doi.org/10.1038/nature06045.

[7] Bladon KD, Silins U, Landhäusser SM, Lieffers VJ. Differential transpiration by three boreal tree species in response to increased evaporative demand after variable retention harvesting. Agric For Meteorol 2006;138(1–4):104–19. http://dx.doi.org/10.1016/j.agrformet.2006.03.015.

[8] Caird MA, Richards JH, Donovan LA. Nighttime stomatal conductance and transpiration in C_3 and C_4 plants. Plant Physiology 2007;143(1):4–10. http://dx.doi.org/10.1104/pp.106.092940.

[9] Campbell GS, Norman J. An introduction to environmental biophysics. New York: Springer; 1998.

[10] Campbell-Clause JM. Stomatal response of grapevines to wind. Anim Prod Sci 1998;38(1):77–82. http://dx.doi.org/10.1071/EA91220.

[11] Chu CR, Hsieh C-I, Wu S-Y, Phillips NG. Transient response of sap flow to wind speed. J Exp Bot 2009;60(1):249–55. http://dx.doi.org/10.1093/jxb/ern282.

[12] Cowan I, Farquhar G. Stomatal function in relation to leaf metabolism and environment. Symposia of the Society for Experimental Biology. Integration of activity in the higher plant, 31. Cambridge: Cambridge University Press; 1977.

[13] Cox P, Betts R, Jones C, Spall S, Totterdell I. Acceleration of global warming due to carbon-cycle feedbacks in a coupled climate model. Nature 2000;408(6809):184–7. http://dx.doi.org/10.1038/35041539.

[14] Damour G, Simonneau T, Cochard H, Urban L. An overview of models of stomatal conductance at the leaf level. Plant Cell Environ 2010;33(9):1419–38. http://dx.doi.org/10.1111/j.1365-3040.2010.02181.x.

[15] Dawson TE, Burgess SSO, Tu KP, Oliveira RS, Santiago LS, Fisher JB, et al. Nighttime transpiration in woody plants from contrasting ecosystems. Tree Physiol 2007;27(4):561–75. http://dx.doi.org/10.1093/treephys/27.4.561.

[16] DeLucia EH, Heckathorn SA. The effect of soil drought on water-use efficiency in a contrasting Great Basin desert and Sierran montane species. Plant Cell Environ 1989;12(9):935–40. http://dx.doi.org/10.1111/j.1365-3040.1989.tb01973.x.

[17] Dixon M, Grace J. Effect of wind on the transpiration of young trees. Ann Bot 1984;53(6):811–19.

[18] Duursma RA, Payton P, Bange MP, Broughton KJ, Smith RA, Medlyn BE, et al. Near-optimal response of instantaneous transpiration efficiency to vapour pressure deficit, temperature and [CO_2] in cotton (*Gossypium hirsutum* L.). Agric For Meteorol 2013;168:168–76. http://dx.doi.org/10.1016/j.agrformet.2012.09.005.

[19] Farquhar GD, von Caemmerer S, Berry JA. A biochemical model of photosynthetic CO_2 assimilation in leaves of C_3 species. Planta 1980;149(1):78–90. http://dx.doi.org/10.1007/BF00386231.

[20] Gates DM. Transpiration and leaf temperature. Annu Rev Plant Physiol 1968;19(1):211–38. http://dx.doi.org/10.1146/annurev.pp.19.060168.001235.

[21] Gedney N, Cox P, Betts R, Boucher O, Huntingford C, Stott P. Detection of a direct carbon dioxide effect in continental river runoff records. Nature 2006;439(7078):835–8. http://dx.doi.org/10.1038/nature04504.

[22] Givnish TJ, Vermeij GJ. Sizes and shapes of liane leaves. Am Nat 1976:743–78. http://dx.doi.org/10.1086/283101.

[23] Grace J. The effect of wind on grasses 1. cuticular and stomatal transpiration. J Exp Bot 1974;25(3):542–51. http://dx.doi.org/10.1093/jxb/25.3.542.

[24] Grace J, Malcolm DC, Bradbury IK. The effect of wind and humidity on leaf diffusive resistance in Sitka spruce seedlings. J Appl Ecol 1975:931–40. http://dx.doi.org/10.2307/2402099.

[25] Grace J, Russell G. The effect of wind and a reduced supply of water on the growth and water relations of *Festuca arundinacea* Schreb. Ann Bot 1982;49(2):217–25.

[26] Granier A. Evaluation of transpiration in a Douglas-fir stand by means of sap flow measurements. Tree Physiol 1987;3(4):309–20. http://dx.doi.org/10.1093/treephys/3.4.309.

[27] Green SR, McNaughton KG, Greer DH, McLeod DJ. Measurement of the increased PAR and net all-wave radiation absorption by an apple tree caused by applying a reflective ground covering. Agric For Meteorol 1995;76(3):163–83. http://dx.doi.org/10.1016/0168-1923(95)02228-P.

[28] Gutiérrez MV, Meinzer FC, Grantz DA. Regulation of transpiration in coffee hedgerows – covariation of environmental variables and apparent responses of stomata to wind and humidity. Plant Cell Environ 1994;17(12):1305–13. http://dx.doi.org/10.1111/j.1365-3040.1994.tb00532.x.

[29] Hari P, Mäkelä A, Korpilahti E, Holmberg M. Optimal control of gas exchange. Tree Physiol 1986;2(1–3):169–75. http://dx.doi.org/10.1093/treephys/2.1-2-3.169.

[30] Huang L, Zhang Z-S, Li X-R. Sap flow of *Artemisia ordosica* and the influence of environmental factors in a revegetated desert area: Tengger Desert, China. Hydrol Process 2010;24(10):1248–53. http://dx.doi.org/10.1002/hyp.7584.

[31] Hunt LA, Impens II, Lemon ER. Preliminary wind tunnel studies of the photosynthesis and evapotranspiration of forage stands. Crop Sci 1967;7(6):575–8. http://dx.doi.org/10.2135/cropsci1967.0011183X000700060006x.

[32] Jones HG. Plants and microclimate: a quantitative approach to environmental plant physiology. Cambridge: Cambridge University Press; 1992.

[33] Juang J, Katul GG, Siqueira M, Stoy P, McCarthy H. Investigating a hierarchy of Eulerian closure models for scalar transfer inside forested canopies. Boundary-Layer Meteorol 2008;128(1):1–32. http://dx.doi.org/10.1007/s10546-008-9273-2.
[34] Katul G, Ellsworth D, Lai C-T. Modelling assimilation and intercellular CO_2 from measured conductance: a synthesis of approaches. Plant Cell Environ 2000;23(12):1313–28. http://dx.doi.org/10.1046/j.1365-3040.2000.00641.x.
[35] Katul GG, Mahrt L, Poggi D, Sanz C. One- and two-equation models for canopy turbulence. Boundary-Layer Meteorol 2004;113(1):81–109. http://dx.doi.org/10.1023/B:BOUN.0000037333.48760.e5.
[36] Katul GG, Manzoni S, Palmroth S, Oren R. A stomatal optimization theory to describe the effects of atmospheric CO_2 on leaf photosynthesis and transpiration. Ann Bot 2010;105(3):431–42. http://dx.doi.org/10.1093/aob/mcp292.
[37] Katul GG, Oren R, Manzoni S, Higgins C, Parlange MB. Evapotranspiration: a process driving mass transport and energy exchange in the soil-plant-atmosphere-climate system. Rev Geophys 2012;50:RG3002. http://dx.doi.org/10.1029/2011rg000366.
[38] Katul GG, Schieldge J, Hsieh C-I, Vidakovic B. Skin temperature perturbations induced by surface layer turbulence above a grass surface. Water Res Res 1998;34(5):1265–74. http://dx.doi.org/10.1029/98WR00293.
[39] Kim D, Oren R, Oishi AC, Hsieh C-I, Phillips N, Novick KA, et al. Sensitivity of stand transpiration to wind velocity in a mixed broadleaved deciduous forest. Agric For Meteorol 2014;187:62–71. http://dx.doi.org/10.1016/j.agrformet.2013.11.013.
[40] Kitaya Y, Shibuya T, Yoshida M, Kiyota M. Effects of air velocity on photosynthesis of plant canopies under elevated CO_2 levels in a plant culture system. Adv Space Res 2004;34(7):1466–9. http://dx.doi.org/10.1016/j.asr.2003.08.031.
[41] Konrad W, Roth-Nebelsick A, Grein M. Modelling of stomatal density response to atmospheric CO_2. J Theor Biol 2008;253(4):638–58. http://dx.doi.org/10.1016/j.jtbi.2008.03.032.
[42] Lai C, Katul G, Oren R, Ellsworth D, Schäfer K. Modeling CO_2 and water vapor turbulent flux distributions within a forest canopy. J Geophys Res: Atmos 2000;105(D21):26333–51. http://dx.doi.org/10.1029/2000JD900468.
[43] Launiainen S, Katul GG, Kolari P, Vesala T, Hari P. Empirical and optimal stomatal controls on leaf and ecosystem level CO_2 and H_2O exchange rates. Agric For Meteorol 2011;151(12):1672–89. http://dx.doi.org/10.1016/j.agrformet.2011.07.001.
[44] Leuning R. A critical appraisal of a combined stomatal-photosynthesis model for C_3 plants. Plant Cell Environ 1995;18(4):339–55. http://dx.doi.org/10.1111/j.1365-3040.1995.tb00370.x.
[45] Liu F, Andersen MN, Jacobsen S-E, Jensen CR. Stomatal control and water use efficiency of soybean (*Glycine max* L. Merr.) during progressive soil drying. Enviro Exp Bot 2005;54(1):33–40. http://dx.doi.org/10.1016/j.envexpbot.2004.05.002.
[46] Mäkelä A, Berninger F, Hari P. Optimal control of gas exchange during drought: theoretical analysis. Ann Bot 1996;77(5):461–7. http://dx.doi.org/10.1006/anbo.1996.0056.
[47] Manzoni S, Vico G, Katul G, Fay PA, Polley W, Palmroth S, et al. Optimizing stomatal conductance for maximum carbon gain under water stress: a meta-analysis across plant functional types and climates. Funct Ecol 2011;25(3):456–67. http://dx.doi.org/10.1111/j.1365-2435.2010.01822.x.
[48] Manzoni S, Vico G, Palmroth S, Porporato A, Katul G. Optimization of stomatal conductance for maximum carbon gain under dynamic soil moisture. Adv Water Res 2013;62:90–105. http://dx.doi.org/10.1016/j.advwatres.2013.09.020.
[49] Martin EV, Clements FE. Studies of the effect of artificial wind on growth and transpiration in *Helianthus annuus*. Plant Physiol 1935;10(4):613. http://dx.doi.org/10.1104/pp.10.4.613.
[50] Masle J, Farquhar GD. Effects of soil strength on the relation of water-use efficiency and growth to carbon isotope discrimination in wheat seedlings. Plant Physiol 1988;86(1):32–8. http://dx.doi.org/10.1104/pp.86.1.32.
[51] Medlyn BE, Dreyer E, Ellsworth D, Forstreuter M, Harley PC, Kirschbaum MUF, et al. Temperature response of parameters of a biochemically based model of photosynthesis. II. A review of experimental data. Plant Cell Environ 2002;25(9):1167–79. http://dx.doi.org/10.1046/j.1365-3040.2002.00891.x.
[52] Monteith JL. Evaporation and environment. In: Proceedings of Symposia of the Society for Experimental Biology, 19; 1965. p. 205–24.
[53] Mott KA, Parkhurst DF. Stomatal responses to humidity in air and helox. Plant Cell Environ 1991;14(5):509–15. http://dx.doi.org/10.1111/j.1365-3040.1991.tb01521.x.
[54] Novick KA, Oren R, Stoy PC, Siqueira MBS, Katul GG. Nocturnal evapotranspiration in eddy-covariance records from three co-located ecosystems in the Southeastern U.S.: implications for annual fluxes. Agric For Meteorol 2009;149(9):1491–504. http://dx.doi.org/10.1016/j.agrformet.2009.04.005.
[55] Prentice IC, Meng T, Wang H, Harrison SP, Ni J, Wang G. Evidence of a universal scaling relationship for leaf CO_2 drawdown along an aridity gradient. New Phytol 2011;190(1):169–80. http://dx.doi.org/10.1111/j.1469-8137.2010.03579.x.
[56] Sellers P, Bounoua L, Collatz G, Randall D, Dazlich D, Los S, et al. Comparison of radiative and physiological effects of doubled atmospheric CO_2 on climate. Science 1996;271(5254):1402. http://dx.doi.org/10.1126/science.271.5254.1402.
[57] Sellers P, Meeson B, Hall F, Asrar G, Murphy R, Schiffer R, et al. Remote sensing of the land surface for studies of global change: Models - algorithms - experiments. Remote Sens Environ 1995;51(1):3–26. http://dx.doi.org/10.1016/0034-4257(94)00061-Q.
[58] Siqueira M, Katul G. Estimating heat sources and fluxes in thermally stratified canopy flows using higher-order closure models. Boundary-Layer Meteorol 2002;103(1):125–42. http://dx.doi.org/10.1023/A:1014526305879.
[59] Vico G, Manzoni S, Palmroth S, Weih M, Katul G. A perspective on optimal leaf stomatal conductance under CO_2 and light co-limitations. Agric For Meteorol 2013;182:191–9. http://dx.doi.org/10.1016/j.agrformet.2013.07.005.
[60] Volpe V, Manzoni S, Marani M, Katul G. Leaf conductance and carbon gain under salt-stressed conditions. J Geophys Res – Biogeosci 2011;116:G04035. http://dx.doi.org/10.1029/2011jg001848.
[61] Wang KY, Kellomaki S, Laitinen K. Acclimation of photosynthetic parameters in Scots pine after three years exposure to elevated temperature and CO_2. Agric For Meteorol 1996;82(1–4):195–217. http://dx.doi.org/10.1016/0168-1923(96)02329-5.
[62] Wullschleger SD. Biochemical limitations to carbon assimilation in C_3 plants – a retrospective analysis of the A/C_i curves from 109 species. J Exper Bot 1993;44(5):907–20. http://dx.doi.org/10.1093/jxb/44.5.907.
[63] Zalesny RS Jr, Wiese AH, Bauer EO, Riemenschneider DE. Sapflow of hybrid poplar (*Populus nigra*L.P. *maximowiczii* A. Henry 'NM6') during phytoremediation of landfill leachate. Biomass Bioenergy 2006;30(8):784–93. http://dx.doi.org/10.1016/j.biombioe.2005.08.006.